HHS Public Access

Author manuscript

Cell Rep. Author manuscript; available in PMC 2020 May 04.

Published in final edited form as:

Cell Rep. 2020 March 31; 30(13): 4490–4504.e4. doi:10.1016/j.celrep.2020.03.027.

Cortical Neural Stem Cell Lineage Progression Is Regulated by Extrinsic Signaling Molecule Sonic Hedgehog

Yue Zhang[1,5], **Guoping Liu**[2,5], **Teng Guo**[2,5], **Xiaoyi G. Liang**[1,5], **Heng Du**[2], **Lin Yang**[2], **Aparna Bhaduri**[3], **Xiaosu Li**[2], **Zhejun Xu**[2], **Zhuangzhi Zhang**[2], **Zhenmeiyu Li**[2], **Miao He**[2], **Jeremiah Tsyporin**[1], **Arnold R. Kriegstein**[3], **John L. Rubenstein**[4], **Zhengang Yang**[2,*], **Bin Chen**[1,6,*]

[1]Department of Molecular, Cell and Developmental Biology, University of California, Santa Cruz, Santa Cruz, CA 95064, USA

[2]State Key Laboratory of Medical Neurobiology and MOE Frontiers Center for Brain Science, Institute for Translational Brain Research, Institutes of Brain Science, Department of Neurology, Zhongshan Hospital, Fudan University, Shanghai 200032, China

[3]Eli and Edythe Broad Center for Regeneration Medicine and Stem Cell Research, University of California, San Francisco, San Francisco, CA 94143, USA

[4]Nina Ireland Laboratory of Developmental Neurobiology, Department of Psychiatry, UCSF Weill Institute for Neurosciences, University of California, San Francisco, San Francisco, CA 94158, USA

[5]These authors contributed equally

[6]Lead Contact

SUMMARY

Neural stem cells (NSCs) in the prenatal neocortex progressively generate different subtypes of glutamatergic projection neurons. Following that, NSCs have a major switch in their progenitor properties and produce γ-aminobutyric acid (GABAergic) interneurons for the olfactory bulb (OB), cortical oligodendrocytes, and astrocytes. Herein, we provide evidence for the molecular mechanism that underlies this switch in the state of neocortical NSCs. We show that, at around E16.5, mouse neocortical NSCs start to generate GSX2-expressing ($GSX2^+$) intermediate progenitor cells (IPCs). *In vivo* lineage-tracing study revealed that $GSX2^+$ IPC population gives rise not only to OB interneurons but also to cortical oligodendrocytes and astrocytes, suggesting that they are a tri-potential population. We demonstrated that Sonic hedgehog signaling is both

*Correspondence: yangz@fudan.edu.cn (Z.Y.), bchen@ucsc.edu (B.C.).

AUTHOR CONTRIBUTIONS

Y.Z., G.L., T.G., and X.G.L. performed most of the experiments and analyzed the data. H.D., Z.X., Z.Z., Z.L., M.H., and J.T. helped with genotyping, graph plotting, and data interpretation. A.B., L.Y., and X.L. analyzed scRNA-seq and RNA-seq results. Z.Y., B.C., J.L.R., and A.R.K. analyzed the data and edited the manuscript. Z.Y. and B.C. designed the study, interpreted the results, and wrote the manuscript.

SUPPLEMENTAL INFORMATION

Supplemental Information can be found online at https://doi.org/10.1016/j.celrep.2020.03.027.

DECLARATION OF INTERESTS

J.L.R. and A.R.K. are cofounders, stockholders, and on the scientific board of Neurona, a company studying the potential therapeutic use of interneuron transplantation. The other authors declare no competing interests.

necessary and sufficient for the generation of GSX2$^+$ IPCs by reducing GLI3R protein levels. Using single-cell RNA sequencing, we identify the transcriptional profile of GSX2$^+$ IPCs and the process of the lineage switch of cortical NSCs.

Graphical Abstract

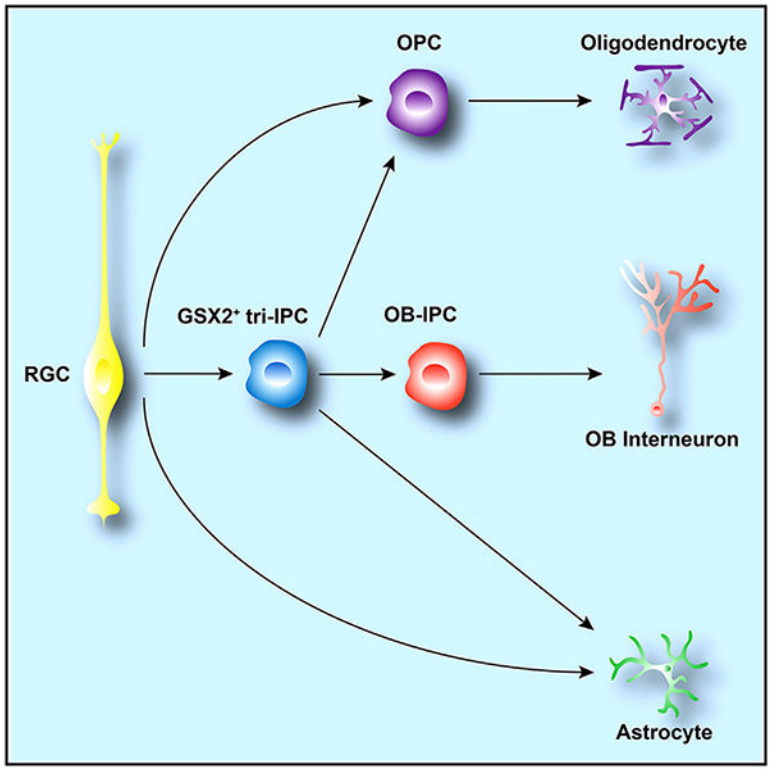

In Brief

Zhang et al. reveal that cortical radial glia-derived GSX2$^+$ cells at the late embryonic stage are tri-potential intermediate progenitors, which give rise to a subset of cortical oligodendrocytes, astrocytes, and olfactory bulb interneurons. SHH signaling is crucial for the generation of GSX2$^+$ cells by reducing GLI3R protein level.

INTRODUCTION

Neural stem cells (NSCs) are the ultimate source of all neurons, oligodendrocytes, and astrocytes. Prenatally, NSCs correspond to radial glial cells (RGCs) that are regionally and temporally specified and generate diverse neuronal and glial cell types appropriate for their location and time (Bayraktar et al., 2014; Kriegstein and Alvarez-Buylla, 2009; Kwan et al., 2012). Although much progress has been made toward understanding temporal cell-fate specification in the developing invertebrate ventral nerve cord and brain (Doe, 2017; Kohwi and Doe, 2013), the mechanisms responsible for temporal lineage specification of NSCs in the mammalian brain remain largely unknown.

The mouse cerebral cortex is a six-layered structure, consisting of both glutamatergic, pyramidal-projection neurons (PyNs) derived from cortical ventricular zone (VZ) and subventricular zone (SVZ), and g-aminobutyric acid (GABAergic) interneurons that arise from subcortical progenitor domains. During development, embryonic NSCs located in the cortical VZ sequentially generate distinct subtypes of PyNs in an inside-out pattern: deep-layer PyNs are born first, followed by PyNs of superficial layers (Kriegstein and Alvarez-Buylla, 2009; Kwan et al., 2012; Leone et al., 2008). The local interneurons, however, derive from NSCs located in the medial and caudal ganglionic eminences (MGEs and CGEs, respectively) in the ventral forebrain and migrate tangentially into the cerebral cortex (Hu et al., 2017; Lim et al., 2018).

As the production of PyNs ceases, cortical NSCs switch to generating cortical glia and GABAergic olfactory bulb (OB) interneurons (Kessaris et al., 2006; Kohwi et al., 2007; Kriegstein and Alvarez-Buylla, 2009; Kwan et al., 2012; Merkle et al., 2007; Ventura and Goldman, 2007; Young et al., 2007). Using time-lapse imaging *in vitro*, we have previously demonstrated that individual embryonic day-11.5 (E11.5) mouse cortical RGCs generate TBR1-expressing ($TBR1^+$) PyNs, followed by GAD1 and SP8 double-positive ($GAD1^+SP8^+$) OB interneurons (OB-INs) (Cai et al., 2013). A recent lineage analysis using barcoded virus libraries confirmed this result and revealed that individual early cortical RGCs generate both PyNs and OB-INs *in vivo* (Fuentealba et al., 2015). Lineage analysis of late embryonic cortical RGCs showed that, although they no longer produce PyNs, they generate cortical astrocytes and oligodendrocytes (Gao et al., 2014; Guo et al., 2013). Thus, cortical RGCs progress from generating PyNs to oligodendrocytes, astrocytes, and OB GABAergic interneurons at the end of cortical neurogenesis. Recently, it has been shown that Sonic hedgehog (SHH) signaling is critical for cortical RGCs to generate oligodendrocytes (Winkler et al., 2018), but the mechanism regulating the switch for cortical RGCs to generate OB-INs is unknown.

Here, we show that at the end of PyN production, cortical NSCs begin generating $GSX2^+$ intermediate progenitor cells (IPCs) in the SVZ. Importantly, we demonstrate that $GSX2^+$ cells are tri-potent IPCs (tri-IPCs) at the population level, giving rise to OB-INs, cortical oligodendrocytes, and astrocytes. We show that SHH signaling is both necessary and sufficient for cortical RGCs to switch from generating PyNs to producing $GSX2^+$ tri-IPCs and OB-INs; this switch requires blocking the formation of the GLI3 repressor (Gli3R) transcription factor. Finally, single-cell RNA sequencing (scRNA-seq) analysis confirms these findings and identifies the molecular signatures of $GSX2^+$ IPCs in the cortex.

RESULTS

GSX2 Is Expressed in a Subpopulation of IPCs in the Cortex

We have recently identified a genetic pathway (*Gsx2/1–Dlx1/2–Sp8/Sp9–Tshz1–Prokr2*) that is crucial for generating virtually all OB-INs (Guo et al., 2019; Li et al., 2018). In this transcriptional cascade, *Gsx2* is at the top of the hierarchy, and its expression and functions in NSCs and IPCs in the lateral ganglionic eminence (LGE) have been well documented (Guo et al., 2019; Toresson and Campbell, 2001; Waclaw et al., 2009; Wang et al., 2013). It is known that a subpopulation of OB-INs is derived from cortical progenitors (Kriegstein

and Alvarez-Buylla, 2009). However, it is unclear whether the above transcription factors are expressed by cortical progenitors. To answer that question, we examined the expression of GSX2 in the cortex.

At E16.5, the time when the production of PyNs ceases, only a few cells in the cortical SVZ weakly expressed GSX2 (Figure 1A). From E17.5 to P21, $GSX2^+$ cells were observed in the cortical SVZ and intermediate zone (Figures 1A and S1A). We analyzed co-expression of GSX2 and MKI67 in the E18.5 cortex and found that 86.1% of $GSX2^+$ cells expressed MKI67 and 30.4% of $MKI67^+$ cells in the SVZ expressed GSX2 (Figures S1B and S1C). This suggests that $GSX2^+$ cells represent a subpopulation of the cycling progenitors in the cortex. Although GSX2 is expressed in NSCs and IPCs in the VZ and SVZ of the LGE (Guo et al., 2019; Wang et al., 2009), we did not observe $GSX2^+$ cells in the cortical VZ, indicating that they are IPCs, rather than the primary VZ RGCs.

We next asked how numerous $GSX2^+$ cells are in the cortex in prenatal and postnatal stages. To address this question, we quantified the numbers of $GSX2^+$ cells in the cortex at E18.5, P1, P3, P5, and P7 in the rostro-caudal and medio-lateral axes (Figures S1D–S1F). In general, $GSX2^+$ cells showed a lateral-to-medial spatial gradient with the numbers of $GSX2^+$ cells highest in the intermediate cortex and fewer in the rostral and caudal cortices at all stages (Figures S1D–S1F). Interestingly, it appeared that there were more cortical $GSX2^+$ cells at P0 and P5 than at other stages (Figure S1F). Taken together, these results suggest that a subset of IPCs in the cortex express GSX2 in the prenatal and postnatal mouse telencephalon.

Eomesodermin (EOMES; TBR2) is a transcription factor of the T-box family expressed by IPCs in the PyN lineage of the cortex (Bulfone et al., 1999; Hevner, 2019; Lv et al., 2019). We did not observe co-expression of GSX2 and EOMES in the cortex (Figures S1D and S1E). The ratios of $GSX2^+$ cells to $EOMES^+$ cells increase with developmental stages from 0.25 at E18.5 to 2.7 at P7 (Figure S1G), as the numbers of $EOMES^+$ cells drop sharply in the postnatal cortex (Kowalczyk et al., 2009).

Cortical NSCs Generate $GSX2^+$ IPCs at Late Embryonic Stages

To determine whether the $GSX2^+$ IPCs in the cortex originated from the cortical VZ or migrated from the LGE, we performed intersectional (IS) analysis using *Cre* and *Flpo* recombinases in combination with an *IS* reporter mouse line (He et al., 2016) (Figure 1B). We generated the $Gsx2^{Flpo}$ allele by inserting a *P2A-Flpo-T2A-Flpo* cassette immediately before the stop codon of the endogenous *Gsx2* gene (Figure S2A). We confirmed the specificity of *Flpo* activity in the $Gsx2^+$ cells by breeding the $Gsx2^{Flpo/+}$ mice with *Rosa26-tdTomato-FRT* mice (He et al., 2016). TdTomato (tdT) expression was observed in the LGE and MGE at E13.5 and E14.5 (Figure S2B), consistent with the expression pattern of GSX2 protein. To perform intersectional lineage analysis, we delivered *pCAG-Cre* plasmids specifically into the cortical VZ of $Gsx2^{Flpo/+}$; *IS* embryos on E14.5 by *in utero* electroporation (IUE). In this experiment, cells generated from electroporated cortical RGCs that did not go through a $Gsx2^+$ stage expressed tdT. On the other hand, cells generated from the electroporated RGCs that did go through a $Gsx2^+$ stage expressed GFP (Figure 1B). We examined the brains at E18.5. The electroporation sites were confirmed by examining tdT

expression (Figure 1C). We observed many tdT^+ cells that extended from the IUE VZ/SVZ to the cortical plate. Fewer GFP^+ cells were observed; most of them were in the cortical SVZ, intermediate zone and some in the cortical plate (Figure 1C). GFP^+ cells were not observed in the cortical VZ. Moreover, the GFP^+ cells in the cortical SVZ did not have a bipolar shape with elongated radial fibers that projected toward the pial surface (Figure 1C), providing evidence that they were not RGCs.

We next analyzed the identities of GFP^+ cells in the E18.5 cortex. We found that 36.4% of GFP^+ cells expressed SP8, 46.9% expressed OLIG2, and only 5.0% expressed GSX2 (Figures S2C–S2G), suggesting that GSX2 is transiently expressed in the IPCs. At E18.5, nearly all $GSX2^+GFP^+$ cells retained tdT expression (Figure S2G) because of the perdurance of the tdT protein. We also observed many cortical RGC-derived tdT^+GSX2^+ cells that did not express GFP (Figure S2G), suggesting a lower recombination efficiency of the *Flp-FRT* system. Taken together, our results demonstrated that the $GSX2^+$ IPCs in the cortex are derived from the cortical RGCs.

Lineage Tracing Reveals the Tri-potency of $GSX2^+$ IPCs in the Cortex

We next examined the lineages of the $GSX2^+$ cortical IPCs. We electroporated *pCAG-Cre* plasmids into the cortical VZ of $Gsx2^{Flpo/+}$; *IS* embryos on E14.5 and analyzed the brains and OBs at P21. We observed many tdT^+ and/or GFP^+ interneurons in the OB; 42.6% of lineage-traced cells were GFP^+, 28.7% tdT^+, and 28.7% of cells expressed both GFP and tdT (Figures 1D and 1E). The GFP^+tdT^+ interneurons in the OB were due to the perdurance of the tdT protein, and these neurons were possibly generated later than the GFP^+-only cells. The total percentage of GFP^+ and GFP^+tdT^+ cells among all the lineage-traced OB-INs were about 71.3%. Although we cannot exclude the possibility that a small number of cortical RGCs directly give rise to OB-INs without going through a $GSX2^+$ IPC stage, this number was likely an underestimate because of the lower recombination efficiency of the *Flp-FRT* system compared with the *Cre-Loxp* system (Buchholz et al., 1998). Thus, most, if not all, of the OB-INs originating from the cortical VZ were the progeny of $GSX2^+$ cortical IPCs.

We also observed a substantial number of GFP^+ cells in the cortex; their morphology and expression of OLIG2 and S100b indicated that these were oligodendrocytes and astrocytes (Figures 1F–1H). The ratio of oligodendrocytes to astrocytes was 6:1 (Figure 1I). These results demonstrated that cortical $GSX2^+$ IPCs give rise not only to interneurons in the OB but also to cortical oligodendrocytes and astrocytes, suggesting that, at the population level, the $GSX2^+$ cells are tri-potent IPCs or tri-IPCs. However, it is unclear whether individual $GSX2^+$ IPCs give rise to all three lineages or the $GSX2^+$ IPCs consist of different uni-potent or bi-potent IPC populations that produce one or two cell lineages.

To confirm our IUE-based lineage-tracing results, we examined $Emx1^{Cre/+}$; $Gsx2^{Flpo/+}$; *IS* triple-transgenic mice in which Cre recombinase was activated in cortical RGCs at approximately E10.5 (Gorski et al., 2002) (Figure S3). At P21, we observed many GFP^+ interneurons in the OB (Figure S3F) and GFP^+OLIG2^+ oligodendrocytes and GFP^+S100b^+ astrocytes in the cortex (Figures S3A–S3C). About 10% of $OLIG2^+$ cells and ~ 4% of $S100b^+$ cells were labeled by GFP (Figure S3D), suggesting that $GSX2^+$ IPCs contribute to small portions of cortical oligodendrocytes and astrocytes. The ratio of oligodendrocytes to

astrocytes among the GFP$^+$ glial cells was ~ 6:1 (84.7% versus 15.3%) (Figure S3E), similar to those observed with the *pCAGIG-Cre* IUE approach (Figures 1F–1I). Together, these results demonstrated that the cortical GSX2$^+$ cell population at late embryonic and early postnatal stages generates OB-INs and both types of cortical glia.

The SHH Signaling Pathway Is Required for the Cortical RGCs to Generate OB-Ins

Neurogenesis in the ventral telencephalon largely generates GABAergic neurons. SHH signaling promotes ventral identities during development throughout the neuroaxis (Hébert and Fishell, 2008). OB-INs production from the dorsal cortex was observed concurrently with increased expression in the cortical VZ/SVZ at P0 and P7 of *Gli1*, which encodes a transcription factor that promotes SHH signaling (Tong et al., 2015). To explore the possibility that OB-IN production requires SHH signaling, we deleted the Smoothened (*Smo*) gene utilizing an *hGFAP-Cre* allele (Zhuo et al., 2001). *Smo* encodes a G-protein-coupled receptor that is an essential signal transducer for the SHH pathway. *hGFAP-Cre* is active in the cortical RGCs from E13.5 and in the LGE and CGE from E16.5.

We compared the expression of OB-IN lineage markers in the *hGFAP-Cre; Smo$^{F/F}$* (*Smo cko*) mice with littermate control *hGFAP-Cre; Smo$^{F/+}$* mice at P2 using *in situ* RNA hybridization and immunohistochemistry (Figure 2). Reduced expression of *Gli1* mRNA confirmed decreased SHH signaling in the cortical VZ/SVZ of *Smo cko* mice (Figure 2A). Almost all GSX2$^+$ cells were lost in the rostral and caudal cortical SVZ (Figures 2B–2D), as were cells expressing OB-IN markers *Sp9*, *Tshz1*, and *Prokr2* and the pan-GABAergic neuron marker *Gad1* (Figure 2A). The number of SP8$^+$ cells in the cortical SVZ was also significantly reduced (Figures 2B–2D); the remaining SP8$^+$ cells in the *Smo cko* cortical SVZ were probably CGE-derived cortical interneurons (Ma et al., 2012).

The lack of OB-INs in the cortical VZ/SVZ of *Smo cko* mice could be due to a defect in fate specification or to reduced cell proliferation. To distinguish between these possibilities, we examined numbers of EOMES$^+$ cells and cell proliferation by administrating EdU to label S-phase cells 2 h before sacrificing the mice. At P0, the number of EdU$^+$ cells in the mutant VZ was not significantly different from that in the control brains. However, in the *Smo cko* SVZ, there were fewer EOMES$^+$ cells, and there was a significant reduction of the EdU$^+$ cells (Figures S4A and S4C). This observation was consistent with a previous report that SHH signaling is not required for cortical RGC proliferation, but rather, it promotes the proliferation of cortical IPCs (Komada et al., 2013). Unlike at P0, by P3, the number of EOMES$^+$ cells was not significantly affected (Figure S4B and S4C). We postulate that the restored EOMES$^+$ IPC cells at P3 likely originated from the cortical RGCs. The reduced OB lineage cells and normal EOMES$^+$ cell number at P3 provide further evidence that SHH signaling drives cortical RGCs to switch from generating EOMES$^+$ IPCs to GSX2$^+$ IPCs and OB-INs.

Increased Exposure to SHH during Neurogenesis of Deep-Layer Pyramidal Neurons Causes a Premature Fate Switch to Generate OB-INs and Oligodendrocytes

Recently, it was reported that SHH signaling promotes cortical RGCs to generate oligodendrocytes (Winkler et al., 2018). Both GSX2$^+$ and OLIG2$^+$ cells appear in the

cortical SVZ around E16.5 during normal development (Figure 1A) (Winkler et al., 2018). Is this because cortical RGCs are exposed to increased SHH signal at the end of cortical neurogenesis or because they become competent to respond to SHH signaling to generate these cell types only at that time? To address those questions, we ectopically expressed SHH in the cortical VZ by electroporating the *pCAG-ShhN-ires-GFP* plasmid into wild-type (WT) mice at E13.5 (the peak time for generating layer-5 cortical projection neurons) and examined the brains at E18.5 (Figure 3A). Controls were electroporated with the *pCAG-GFP* plasmid. Brains electroporated with the *pCAG-ShhN-ires-GFP* had increased *Gli1* and *Ptch1* expression, consistent with increased activation of the SHH signaling pathway (Figure 3A) (Shikata et al., 2011). Furthermore, more cells expressed OB-IN lineage markers: GSX2, ASCL1, DLX2, SP8, SP9, *Tshz1*, *Prokr2*, and *Gad1* (Figures 3A and 3B). The number of $OLIG2^+$ cells also increased (Figure 3B), consistent with a previous report (Winkler et al., 2018). Bulk RNA-seq analysis confirmed the increased expression of genes associated with OB-INs (*Gsx2*, *Ascl1*, *Dlx1/2*, *Gad1*, *Sp8/9*, *Tshz1*, and *Prokr2*) and oligodendrocytes (*Olig1/2*, *Pdgfra*, and *Sox10*) in the cortices electroporated with *pCAG-ShhN-ires-GFP* at P0 (Figure 3C). Thus, cortical RGCs can respond to increased SHH signaling to generate OB-INs and oligodendrocytes even during the peak time of producing PyNs.

We also investigated the effect of increased SHH pathway activation on OB-IN generation using the conditional $Rosa26^{SmoM2}$ allele, which, upon CRE-mediated recombination, expresses a constitutively active SMO protein, independent of SHH (Jeong et al., 2004). We examined the cortex of *hGFAP-Cre*; $Rosa26^{SmoM2/+}$ and littermate control mice ($Rosa26^{SmoM2/+}$) at E17.5. Similar to SHH overexpression, in *hGFAP-Cre*; $Rosa26^{SmoM2/+}$ mice we observed increased the numbers of cells expressing OB-IN and oligodendrocyte lineage markers (Figure S5A–S5C). Most PyNs are generated between E11.5 and E16.5 in the neocortex. Our RNA-seq data from the P0 cortex of *hGFAP-Cre*; $Rosa26^{SmoM2/+}$ mice showed mis-regulation of many genes associated with PyNs (Figure S5D). Consistently, misregulated PyN gene expression in the *Shh-IUE* cortex was also observed at P0 (Figure S5E). These results indicate that cortical PyN development is compromised after overexpression of *ShhN* or *SmoM2* at E13.5 (Yabut et al., 2015).

SHH Signaling Promotes OB-IN and Cortical Oligodendrocyte Fates through Reducing GLI3R

Both *Gli2* and *Gli3* have been shown to mediate the downstream signaling of SHH; GLI2 can both activate (GLI2A) and repress (GLI2R) gene expression, whereas GLI3 acts mostly as a transcription repressor (Gli3R) (Hui and Angers, 2011). *Gli2* and *Gli3* are expressed in the cortical VZ/SVZ throughout embryonic development (Sousa and Fishell, 2010) and in the SVZ of the lateral ventricle postnatally (Petrova et al., 2013; Wang et al., 2014). To determine whether the SHH pathway promotes cortical RGCs to generate $Gsx2^+$ IPCs through activating GLI2A or through reducing GLI3R, we examined the brains of *hGFAP-Cre;* $Gli2^{F/F}$ (*Gli2 cko*) (Corrales et al., 2006), *hGFAP-Cre;* $Gli3^{F/F}$ (*Gli3 cko*) (Blaess et al., 2008), and *hGFAP-Cre;* $Gli2^{F/F}$; $Gli3^{F/F}$ (*Gli2 Gli3 dcko*) mice at P0 (Figures 4A–4D). Compared with the WT mice, the numbers of $GSX2^+$, $SP8^+$, and $OLIG2^+$ cells were not significantly affected in the *Gli2 cko* mice (Figure 4E), but their numbers were significantly

increased in cortical VZ/SVZ of the *Gli3 cko* mice (Figures 4C and 4E). These results suggested that *Gli2* is not required for the lineage switch, whereas *Gli3* inhibits the cortical RGCs from generating OB-INs and oligodendrocytes. Consistent with that, significantly more GSX2$^+$, SP8$^+$, and OLIG2$^+$ cells were present in the cortical VZ/SVZ of the *Gli2 Gli3 dcko* than in the WT brains (Figure 4E).

We next examined the brains of *hGFAP-Cre; Smo$^{F/F}$; Gli3$^{F/F}$* (*Smo Gli3 dcko*) mice. Although the numbers of GSX2$^+$, SP8$^+$, and OLIG2$^+$ cells were reduced in the *Smo cko* mice (Figures 2B–2D, 4B, and 4E), they were restored in the *Smo Gli3 dcko* mice. Compared with the WT, more GSX2$^+$, SP8$^+$, and OLIG2$^+$ cells were observed in the cortical VZ/SVZ of *Smo Gli3 dcko* mice at P0 (Figures 4D and 4E). These results indicate that GLI3 inhibits cortical RGCs from generating OB-INs and oligodendrocytes, and that SHH pathway activation blocks this inhibition to enable the production of those cell lineages.

We analyzed neurogenesis in the adult SVZ (P90). Whole mount of the lateral wall of lateral ventricle stained with antibody against DCX showed a marked decrease in neuroblast chains in *Smo cko* mice (Figure S4D), but this defect was largely rescued in *Smo Gli3 dcko* mice (Figure S4D). Thus, GLI3 also inhibits neurogenesis of OB-INs in the adult SVZ.

scRNA-Seq Analysis Supports the Existence of Gsx2$^+$ Tri-IPCs in the Developing Cortex

We performed scRNA-seq to analyze the cortical progenitors undergoing the lineage switch. Neocortices from E16.5 WT mice (*wt* sample) and from E16.5 cortices that were electroporated with *pCAG-ShhN-ires-GFP* plasmids on E13.5 (*ShhN-IUE* sample) were dissected, dissociated into single-cell suspensions, and sequenced using the 103 genomics platform. After removing outlier cells that had a high percentage of ribosomal or mitochondrial genes, 7,494 cells in the *wt* sample and 8,311 cells in the *ShhN-IUE* sample were used for analysis, with an average of 2,450 genes detected per cell (Figures 5A and 5B).

After confirming no batch effect between the two samples, dimensionality reduction followed by unsupervised clustering using Louvian community detection (Blondel et al., 2008) and visualization with t-Distributed Stochastic Neighbor Embedding (t-SNE) (Macosko et al., 2015) revealed 31 clusters in the *wt* sample (Figure S6) and 36 clusters in the *ShhN-IUE* sample (Figure S7). Gene ontology analysis classified those clusters into discrete populations, including RGCs, IPCs, PyNs, cortical interneurons (CINs), endothelial cells (ECs) and microglia, and Cajal-Retzius cells (CRs) (Figure 5A). In the *ShhN-IUE* sample, we identified additional clusters with molecular signatures of tri-IPCs, oligodendrocyte progenitor cells (OPCs), and OB-IN IPCs (OB-IPCs) that were not identified in the *wt* sample (Figures 5A, 5B, S6, and S7). This was likely due to the small numbers of tri-IPCs, OPCs, and OB-IPCs present in the WT cortical SVZ at E16.5. Indeed, we observed only 8 *Gsx2*$^+$ (0.10% of the population) and 27 *Olig2*$^+$ (0.36%) progenitor cells in the *wt* sample, whereas there were 214 *Gsx2*$^+$ (2.57%) and 222 *Olig2*$^+$ (2.67%) progenitor cells after *ShhN*-IUE (Figures 5C and 5D). Five days after *ShhN*-IUE, we observed *Tshz1*$^+$ and *Prokr2*$^+$ OB immature interneurons in the E18.5 cortices by *in situ* RNA hybridization (Figure 3A), but we did not find *Tshz1*$^+$ and *Prokr2*$^+$ cells 3 days after *ShhN*-IUE in the E16.5 cortices in our scRNA-seq results. This is likely due to the OB-IPCs

not having enough time to differentiate into postmitotic OB-INs at E16.5. An astrocyte cluster was not identified at this time; astrocytes are generated mainly after PyN neurogenesis.

The gene regulatory network *Gsx2/1–Dlx1/2–Sp8/Sp9–Tshz1–Prokr2* is crucial for the generation and differentiation of virtually all OB-INs, and the homeobox transcription factor genes, *Dlx1/2*, are central and essential components in this transcriptional code (Guo et al., 2019; Li et al., 2018). Previous fate mapping studies demonstrated that *Dlx1/2-Cre* and *Dlx5/6-Cre* only label neurons, but not oligodendrocytes or astrocytes (Potter et al., 2009; Stenman et al., 2003), strongly suggesting that once IPCs express *Dlx* family genes, their neuronal fate has been determined. It is also known that GSX2 and DLX2 repress OPC specification (Chapman et al., 2013, 2018; Petryniak et al., 2007). Therefore, the IPCs that expressed GSX2 and DLX2/1 were most likely OB-IPCs, even though some of them also expressed OLIG2. In contrast, those IPCs that expressed GSX2 and OLIG2/1, but not DLX2/1, were likely tri-IPCs, with the potential to give rise to either OB-INs or cortical glia or both. Indeed, among the eight *Gsx2*$^+$ cells in the *wt* sample, four cells expressed *Dlx2/1* and *Dcx* (two of them also expressed OLIG2/1) and were OB-IPCs (Figure 5E). The other four *Gsx2*$^+$ cells expressed *Olig2/1*, but not *Dlx2/1*, and were likely tri-IPCs (Figure 5E); they may have the potential to generate oligodendrocytes, astrocytes, and/or OB-INs (Figure 1).

Trajectory analysis using Monocle 2 (Qiu et al., 2017a, 2017b) on all the cells in the *wt* or the *Shh-IUE* sample was unsuccessful, likely because too many clusters were included. Thus, we focused our analysis on the progenitor cells. Louvian analysis of all the progenitor cells in the *ShhN-IUE* sample revealed seven clusters (Figures 6A and 6 B). Based on gene expression patterns, we identified them as RGCs (Dbi$^+$Aldoc$^+$Slc1a3$^+$Gli3$^+$), OB-IPCs (Ascl1$^+$Dlx1$^+$Dlx2$^+$Sp9$^+$), neuroblasts for OB-INs (Dcx$^+$Dlx5$^+$Gad1$^+$Sp8$^+$), OPCs (Olig1$^+$Pdgfra$^+$Sox8$^+$Sox10$^+$), differentiating PyNs (PyNs) (Sox11$^+$Neurod6$^+$Pou3f1$^+$Satb2$^+$), and tri-IPCs (Hes6$^+$Btg2$^+$Gsx2$^+$Olig2$^+$) (Figures 6A–6C). t-SNE visualization (Figures 6A and 6C) showed that cells of the OB-IN lineage and the oligodendrocyte lineage were clearly segregated, exhibiting distinct molecular signatures. Monocle analysis predicted a developmental trajectory and pseudo-time-line progression of the progenitor clusters in the *ShhN-IUE* sample (Figures 6D and 6E). The lineage progression was predicted to start from RGCs passing through tri-IPCs; after which, two distinct trajectories were identified that led to either OPCs or OB-IPCs (Figure 6E). The tri-IPC population was located between RGCs and the OPCs and OB-IPCs, suggesting that tri-IPCs were a transitional cell type that generated OPCs and OB-IPCs, consistent with the lineage-tracing results (Figures 1C–1G).

In Vivo Validation of Markers of Tri-IPCs and Their Lineage Progression in the Cortical SVZ

To further validate the molecular signatures of IPCs identified from the scRNA-seq analysis, we performed triple-immunostaining to examine expressions of GSX2, OLIG2, DLX2, SP9, and SP8 in the E17.0 WT and *ShhN*-IUE cortices. Few GSX2$^+$ cells were observed in the WT cortex (Figure 7A). Compared with the GSX2$^+$ cells, more OLIG2$^+$ cells were observed (Figure 7A), with some of them derived from the LGE and MGE (Kessaris et al., 2006).

There were many $DLX2^+$, $SP9^+$, and $SP8^+$ cells in the cortical SVZ; they were MGE- and/or CGE-derived cortical interneurons (Figures 7A and 7B) (Anderson et al., 1997; Liu et al., 2019; Ma et al., 2012). Although very rare in the E17.0 wt cortex, $GSX2^+OLIG2^+DLX2$ tri-IPCs (arrows in Figure 7A) and some $GSX2^+DLX2^+$ OB-IPCs (arrowheads in Figure 7A) were observed. In the E17.0 *ShhN*-IUE cortex, there were significant increases in the numbers of $GSX2^+$, $OLIG2^+$, $DLX2^+$, $SP9^+$, and $SP8^+$ cells in the VZ and/or SVZ compared with WT mice (Figures 7B–7E). Consistent with the scRNA-seq results, significantly more $GSX2^+$ $DLX2^+$ OB-IPCs and $GSX2^+$ $OLIG2^+$ DLX2 tri-IPCs were present (Figure 7F). Very few IPCs expressed GSX2 alone (Figure 7F). Almost all $GSX2^+$ cells segregated into either tri-IPCs or OB-IPCs, based on the expression of DLX2.

A careful examination of the *ShhN-IUE* cortices revealed that, based on the position of $GSX2^+$ cells closer to the cortical VZ, GSX2 expression began before DLX2, and DLX2 expression began before SP8/9 (Figure 7G), indicating a developmental progression along the OB-IN lineage: $GSX2^+$ tri-IPCs generate $DLX2^+$ OB-IPCs, which, in turn, generate $SP9^+$ and $SP8^+$ OB neuroblasts in the cortical SVZ. This observation supports our unsupervised trajectory analysis results (Figures 6D and 6E) and is consistent with the process of OB-IN development in the dorsal LGE (Guo et al., 2019).

DISCUSSION

In this study, we show that the genetic program *Gsx1/2–Dlx1/2–Sp8/9–Tshz1–Prokr2* is activated in the cortical SVZ at the end of cortical neurogenesis, and we uncover an extrinsic signaling pathway that regulates the lineage switch of cortical NSCs to generate OB-INs. Using loss-of-function and gain-of-function analyses, we show that activation of the SHH pathway is both necessary and sufficient for OB-IN generation in the cortical VZ/SVZ through reducing GLI3R. Blocking SHH signaling by deleting *Smo* leads to reduced production of OB-IN lineage, whereas ectopic activation of the SHH pathway by over-expressing *ShhN* or expressing the *SmoM2* allele leads to an early and over-production of OB-INs and cortical oligodendrocytes. Furthermore, lineage-tracing and scRNA-seq analysis reveal that $GSX2^+$ cells derived from the cortical NSCs are tri-IPCs at the population level; they produce not only interneurons in the OB but also oligodendrocytes and astrocytes in the cortex. These findings reveal the mechanism by which RGC switch their lineage from production of cortical excitatory neurons to the generation of cortical oligodendrocytes, astrocytes, and inhibitory OB-INs.

Cortical NSCs, PyN-IPCs, Tri-IPCs, OPCs, OB-IPCs, Glia-IPCs, and Their Lineage Progression

Generating the diverse neuronal and glial cell types in the mammalian brain is a complex and highly regulated process. Shortly after neural tube closure, NSCs are spatially patterned into discrete progenitor domains. The spatially patterned NSCs undergo sequential neurogenesis and gliogenesis to generate the diverse neuronal and glial cell types (Kriegstein and Alvarez-Buylla, 2009; Kwan et al., 2012). NSCs change their lineage and generate different types of neurons and glial cells based on the developmental stages. In the cerebral cortex, early multipotent cortical RGCs first generate deep-layer PyNs, followed by upper-

layer PyNs. At the end of cortical neurogenesis around E16.5, RGCs switch lineages and produce cortical oligodendrocytes, astrocytes, and OB-INs (Fuentealba et al., 2015; Kriegstein and Alvarez-Buylla, 2009).

Although some PyNs are directly derived from RGCs and some RGCs can directly transform into astrocytes, it is worth noting that most neurons, oligodendrocytes, and astrocytes are not the direct progeny of NSCs but, instead, originate from IPCs (Kriegstein and Alvarez-Buylla, 2009). During the period of cortical neurogenesis around E11.5–E16.5, RGCs undergo asymmetric cell division to self-renew and to produce $EOMES^+$ PyN-IPCs (Englund et al., 2005; Noctor et al., 2004), which exclusively generate PyNs (Lv et al., 2019; Mihalas et al., 2016; Vasistha et al., 2015). During late embryonic and postnatal stages in the mouse cortex, NSC lineage progression becomes complicated, and several distinct IPC populations emerge and coexist in the mouse cortex. OPCs are committed to the oligodendrocyte lineage, whereas OB-IPCs are committed to the OB-IN lineage. Astrocyte-IPCs still remain to be identified. Although *in vitro* studies have shown the existence of bi-potent glia-IPCs (O-2A cells) that give rise to both oligodendrocytes and astrocytes (Raff et al., 1983), this has not been confirmed *in vivo* during development.

In the present study, we used intersectional lineage tracing and scRNA-seq analysis to provide evidence for the existence of $GSX2^+$ tri-IPCs and glia-IPCs in the cortex at the population level during development. These tri-IPCs give rise to OB-IPCs, which generate interneurons that migrate into OB through the rostral migratory stream. In addition, they produce a subset of glia-IPCs, which, in turn, generate OPCs and astrocytes in the cortex (Figures 6D and 6E). We emphasize that it remains to be determined whether single $GSX2^+$ cells proliferate and differentiate into more than one cell type or whether the $GSX2^+$ cells represent a heterogenous population consisting of uni-potential and/or bi-potent neuronal and glial IPCs. Thus, careful analyses of complete lineages of cortical RGCs and IPCs that include their OB-IN progenies need to be performed.

SHH Signaling Promotes the Generation of OB-INs and Cortical Oligodendrocytes by Reducing Gli3R

SHH activity shows a ventral-high and dorsal-low gradient in the VZ of developing forebrain because of the high expression of SHH from ventral cells and the high expression of GLI3R in the dorsal progenitors (Hébert and Fishell, 2008; Sousa and Fishell, 2010). Regulated SHH signaling and GLI activities are essential for the initial dorsal-ventral patterning of the forebrain and the development of cortical interneurons from the ventral forebrain. Ventral forebrain structures are missing in the $Shh^{-/-}$ mice (Ohkubo et al., 2002). Loss of *Gli3* function in *extra-toes* mice (*Gli3* mutants) resulted in ventralization of the cerebral cortex: genes normally expressed in the cerebral cortex were lost; instead, genes associated with ventral and GABAergic neuronal identities were expressed in the dorsal telencephalon (Rallu et al., 2002; Theil et al., 1999; Tole et al., 2000).

Here, we show that the lineage progression of cortical RGCs at late gestational stages is regulated by SHH signaling. During early cortical neurogenesis, RGCs with high GLI3R activity generate $EOMES^+$ PyN-IPCs. Interneurons tangentially migrating from the MGE and CGE, start to arrive the cortex around E13.5, and their numbers continue to increase

(Lim et al., 2018). As cortical neurogenesis proceeds, SHH secreted from migrating cortical interneurons and cells in the choroid plexus (Winkler et al., 2018) promotes the lineage switch of cortical RGCs to generate OB-INs and oligodendrocytes. Indeed, increased numbers of OB-IN and oligodendrocyte lineage cells were observed in the cortical VZ/SVZ of the *ShhN-IUE* and the *hGFAP-Cre; SmoM2* mice (Figures 3 and S5). In contrast, generation of both OB-IN and oligodendrocyte lineage cells from the cortical NSCs was reduced in the *hGFAP-Cre; Smo cko* mice (Figure 2) (Winkler and Franco, 2019; Winkler et al., 2018). Long-term blocking of SHH signaling also resulted in a severe loss of NSCs and migrating neuroblasts in the adult SVZ (Figure S4D) and RMS (Balordi and Fishell, 2007). Significantly, removing *Gli3* in *hGFAP-Cre; Smo cko* mice largely rescued OB-IN genesis and $OLIG2^+$ cell production in the cortex (Figure 4). Hence, SHH promotes the lineage switch of cortical RGCs to generate OB-INs and cortical oligodendrocytes by reducing GLI3R, rather than by directly promoting the GLI activator function, similar to their functions in neurogenesis in the postnatal SVZ and OB (Figure S4D) (Petrova et al., 2013; Wang et al., 2014).

Upon increased SHH signaling, GLI3R protein levels in some cortical RGCs decrease, allowing those RGCs to generate $GSX2^+$ and $OLIG2^+$ IPCs. How does GLI3R repress *Gsx2* expression in the cortical VZ/SVZ? Previous studies have shown that expression of *Dmrta2* (*Dmrt5*), *Dmrt3*, *Emx1*, and *Emx2* in the cortical VZ was severely downregulated in *Gli3* mutant mice (Hasenpusch-Theil et al., 2012; Hasenpusch-Theil et al., 2018; Theil et al., 1999). A recent study demonstrated that transcription factors DMRTA2, DMRT3, and EMX2 cooperatively repress *Gsx2* expression to maintain cortical identity of the RGCs (Desmaris et al., 2018). Furthermore, DMRTA2, DMRT3, and EMX2 have been shown to bind to a ventral telencephalon-specific enhancer in the *Gsx2* locus (Desmaris et al., 2018). Thus, GLI3R could be key to maintaining the expression of *Dmrta2*, *Dmart3*, and *Emx2* in the cortical VZ during early neurogenesis and to preventing expression of *Gsx2*.

A Core Gene Regulatory Network Governing a Common Developmental Trajectory for Forebrain NSCs to Generate OB-Ins

The OB is the most anterior structure of the forebrain. Studies of neurogenesis in the OB have focused on the generation of the OB-INs, in particular, the postnatal and adult neurogenesis occurring in the mouse SVZ of the lateral walls of the lateral ventricle (Obernier and Alvarez-Buylla, 2019). Although NSCs in different domains along the lateral ventricle generate distinct types of neurons and glial cells during embryonic stages, a common trajectory of forebrain NSCs is to switch lineages to generate OB-INs at late embryonic and early postnatal stages (Kriegstein and Alvarez-Buylla, 2009; Obernier and Alvarez-Buylla, 2019).

We recently identified a gene regulatory network *Gsx1/2–Dlx1/2–Sp8/Sp9–Tshz1–Prokr2* that governs OB-IN development; mutations in *Gsx2/1*, *Dlx1/2*, *Sp8/Sp9*, or *Prokr2* genes result in an almost complete loss of mature OB-INs (Guo et al., 2019; Long et al., 2007; Wen et al., 2019). Furthermore, a recent study demonstrated that DLX1 and DLX2 can directly bind to the enhancers and promotors of *Sp8* and *Sp9* (Lindtner et al., 2019). Consistent with the essential regulatory function by this genetic pathway in OB-IN

development, in the present study, we found that this genetic program is activated in cortical progenitors and their progenies when OB-INs are generated. Thus, in addition to functioning in the dorsal LGE during development, this core genetic program regulates the generation of OB-INs from all postnatal NSCs in the ventricular wall of the lateral ventricle.

STAR⋆METHODS

LEAD CONTACT AND MATERIALS AVAILABILITY

Further information and requests for resources and reagents should be directed to and will be fulfilled by the Lead Contact, Dr. Bin Chen (bchen@ucsc.edu). The *Gsx2*-Flpo mouse line will be deposited to the Jackson Laboratory. All unique/stable reagents generated in this study are available by contacting the Lead Contact, but we may require a payment and/or a completed Materials Transfer Agreement if there is potential for commercial application.

EXPERIMENTAL MODEL AND SUBJECT DETAILS

All experiments were performed according to protocols approved by the Institutional Animal Care and Use Committee at University of California at Santa Cruz, and were performed in accordance with institutional and federal guidelines. Experiments performed at Fudan University were in accordance with institutional guideline.

We generated $Gsx2^{Flpo}$ allele by inserting a *P2A-Flpo-T2A-Flpo* DNA cassette between the protein coding sequences of exon 2 and 3′UTR of the *Gsx2* gene (Figure S2A), using a CRISPR/Cas9 based strategy. The sgRNA, the targeting vector and Cas9 were injected into C57BL/6 zygotes to generate founder mice. Founders were screened by PCR to detect integration of the targeting vector. Genomic DNA from mice with positive integration was used to amplify the integration junction for confirmation by sequencing the PCR products. Finally, southern hybridizations using both a *Flpo* probe and a 3′-probe were performed to confirm the correct targeting.

The generation and genotyping of the *Rosa26-tdTomato-FRT* (He et al., 2016), *IS* reporter (JAX no. 028582), $Emx1^{Cre/+}$ (JAX no. 005628), Smo^{FlF} (JAX no. 004526), $Rosa26^{SmoM2/+}$ (JAX no. 005130), $Gli2^{F/F}$ (JAX no. 007926), $Gli3^{F/F}$ (JAX no. 008873), and *hGFAP-Cre* (JAX no. 004600) mice were described previously. The $Gli2^{F/F}$ and $Gli3^{F/F}$ mice were generously provided by Dr. Alexandra Joyner at the Sloan Kettering Institute.

The day of the vaginal plug detection was designated as E0.5. The day of birth was designated as P0. The genders of the embryonic and early postnatal mice were not determined. Both male and female P21 $Gsx2^{Flpo/+}$; *IS* mice and adult $Smo^{fl/fl}$, *Smo cko*, *Gli3 cko*, *Smo Gli3 dcko* mice (P90) were used.

METHOD DETAILS

Immunohistochemistry—Immunohistochemistry was performed using standard protocols. Brains were cryosectioned into thickness of 10 mm, 12 mm, 20 mm or 30 mm. Sections were first permeabilized with 0.05% Triton X-100 for 30 min, followed by an incubation in blocking buffer (5% donkey serum and 0.05% Triton X-100 in TBS) for 2 h. The blocking buffer was removed, and the sections were incubated with primary antibodies

(diluted in the blocking buffer) overnight at 4° C. The following primary antibodies were used in this study: GFP (Chicken, Aves Labs GFP-1020), tdTomato (Goat, SICGEN Ab8181), GSX2 (Rabbit, Millipore ABN162), ASCL1 (Rabbit, Cosmo Bio SKT01–003), SP8 (Goat, Santa Cruz Biotechnology Sc-104661), SP9 (Zhang et al., 2016), DLX2 (Guo et al., 2019; Kuwajima et al., 2006), MKI67 (Mouse, BD Pharmingen 556003), OLIG2 (Rabbit, Millipore AB9610; Mouse, Millipore MABN50) and EOMES (Rat, Thermo Fisher 12-4875-82). The sections were washed in TBS, and incubated with secondary antibodies conjugated to Alexa Fluor488, Cy2, Cy3 or Cy5 for 1.5 h at room temperature. Secondary antibodies were from Jackson ImmunoResearch and Invitrogen. Finally, the sections were counter-stained with DAPI for 3 mins before being mounted in the fluorescence mounting medium (DAKO S3023).

In Situ RNA Hybridization—All *in situ* RNA hybridization assays were performed using digoxigenin riboprobes on 20 mm cryostat sections as previously described (Guo et al., 2019; Zhang et al., 2016).

Digoxigenin-labeled riboprobes used in this study were made from cDNAs amplified by PCR using primers listed in the table.

Probe	Primer Fwd	Rev
Smo	ACATGCCCAAGTGTGAGAATGACC	GCTCTTGATGGAGAACAGAGTCAT
Ptch1	AAGCCCATCGACATTAGTCAGT	ATAAGAGGACAGGCAGCAGAAC
Gli1	TGGAGAACCTTAGGCTGGATCAGC	GGATCAGGATAGGAGACCTGCTGG
Gad1	ATGGCATCTTCCACTCCTTCG	TTACAGATCCTGACCCAACCTCTC
Sp9	ACCTGAATCGTGATTCCCAGCAG	TGCTATGGCTTTTGCAACCCAC
Tshz1	GAGAAGGTCACGGGCAAGGTCAGC	GAGGCGAGGACACAGCATCTGCCA
Prokr2	ATGGGACCCCAGAACAGA	ATGGGACCCCAGAACAGA

EdU labeling—P0 or P3 pups were injected with EdU (50 ug/kg body weight) two h before brain collection. EdU was detected using the Click-iT EdU Cell Proliferation Kit for Imaging (Thermofisher, USA), following the manufacturer's instruction.

Image acquisition and analysis—Images for quantitative analyses were acquired with a Zeiss 880 confocal microscope. Cell counting was performed on single z-slices. Bright field images were acquired with an Olympus BX51 microscope with Q-imaging Ratiga camera. The unpaired t test was used to determine statistical significance.

Analyses were done using GraphPad Prism 5.0, Microsoft Excel and R language. The numbers of GFP^+ or/and tdT^+ cells in the OB, and GFP^+ oligodendrocytes and astrocytes in the cortex (0.40 mm^2 area for the OB and 1.10 mm^2 area for the cortex) were quantified in 3–4 randomly chosen 30 mm sections for P21 *Gsx2*$^{Flpo/+}$; *IS*; *pCAG-Cre* IUE@E14.5 mice. The numbers of $S100b^+$, GFP^+ $S100b^+$, $OLIG2^+$ and GFP^+ $OLIG2^+$ cells in the cortex (0.67mm^2 area) were quantified in 4 randomly chosen 30 mm sections for P21 *Emx1-Cre;* *Gsx2*$^{Flpo/+}$; *IS* mice. The numbers of GFP^+ oligodendrocytes and astrocytes in the cortex

(1.78 mm^2 area) were quantified in 4 randomly chosen 30 mm sections for P21 *Emx1-Cre; Gsx2$^{Flpo/+}$*; *IS* mice, and the percentages of the oligodendrocytes and astrocytes among all GFP^+ cells in the cortex were calculated.

$GSX2^+$ and $EOMES^+$ cells in the entire cortex were quantified in 2 randomly chosen 10 mm sections at rostral, intermediate, and caudal telencephalic levels, respectively, from wild-type mice. The numbers of $GSX2^+$ cells and $SP8^+$ cells in the P2 cortices were counted in 3 randomly chosen 12 mm sections for each group of mice. Two or three brains for each genotype at each stage were used.

For Figures 4 and S4, confocal images were used for quantifying the numbers of $GSX2^+$, $SP8^+$, $EOMES^+$, $OLIG2^+$, EdU^+, and $EOMES^+EdU^+$ cells in the cortical VZ/SVZ in the P0 and P3 brains. The numbers of cells in a 300 mm width were counted. Three sections from each brain, and three brains for each genotype at each stage were used.

Cloning of the pCAG-ShhN-ires-GFP expression plasmid—The *ShhN* cDNA was cloned from *pcDNA3.1-ShhN* plasmid (Addgene # 37680) and inserted into *pCAGGS-ires-EGFP* vector, using NotI and XhoI restriction sites. DNA-sequencing was performed to make sure no mutation was generated during the cloning.

In utero electroporation—*In utero electroporation* (IUE) of wild-type or *Gsx2^{Flpo}; IS* embryos was performed at E13.5 or E14.5. Plasmids *pCAG-Cre* (Addgene #13775), *pCAG-GFP* (Addgene #11150), *pCAG-ShhN-Ires-GFP*, or *pCAG-GFP* (final concentration of 1–2 mg/ml, 0.5ml each embryo) were mixed with 0.05% Fast Green (Sigma), and injected into the lateral ventricle of embryos using a beveled pulled glass micropipette. Five electrical pulses (duration: 50 ms) were applied at 31V for E13.5 embryos and 35V for E14.5 embryos across the uterine wall with a 950 ms interval between pulses. Electroporation was performed using a pair of 7 mm platinum electrodes (BTX, Tweezertrode 45–0488, Harvard Apparatus) connected to an electroporator (BTX, ECM830). Embryos were analyzed at different time points.

RNA-Seq—The P0 cortices from *Rosa26$^{SmoM2/+}$* (control) brains, *hGFAP-Cre; Rosa26$^{SmoM2/+}$* and *ShhN-IUE* (*pCAG-ShhN-Ires-GFP* were electroporated into the wild-type cortex at E13.5) (n = 3 each group) were dissected, and total RNA was isolated with the Direct-zol RNA Miniprep kit (Zymo, catalog #R2050) following the manufacturer's instructions. The gene expression level was reported with fragments per kilobase of exon model per million mapped reads (FPKM) (Trapnell et al., 2012). Genes with a p value <0.05 would be called as differentially expressed.

scRNA-Seq library preparation—*pCAG-ShhN-Ires-GFP* plasmids were electroporated into the cortical VZ of wild-type mice at E13.5. Three days after ShhN-IUE (E16.5), embryos were quickly taken, and the brains were immediately removed and submerged in fresh ice-cold HBSS (GIBCO 14175–095). E16.5 wild type and *ShhN*-IUE cortices were carefully dissected under a fluorescent stereoscope, and incubated in 4 ml of papain solution (final con. 12 U/mL, diluted in DMEM/F-12, Gibco 11330032) for 20 min at 37 C, The

cortical tissues were gently triturated, filtered through a 40 um cell strainer, and washed with HBSS to obtain the single cell suspension.

The Chromium droplet-based sequencing platform (10X Genomics) was used to generate scRNA-Seq libraries, following the manufacturer's instructions (manual document part number: CG00052 Rev C). The cDNA libraries were purified, quantified using Agilent 2100 Bioanalyzer, and sequenced on the Illumina Hiseq4000.

scRNA-Seq analysis—High quality sequences (Clean reads) were obtained by removing low quality sequences and joints. Clean reads were then processed with Cell Ranger software to obtain quantitative information of gene expression and cell population classification. The cell statistical results are shown in the following table.

Group	ShhN-IUE	Wild-type
Estimated Number of Cells	8538	7834
Mean Reads Per Cell	50946	55069
Total Genes Detected	18151	18001
Median Genes Per Cell	2422	2368
Fraction Reads in Cells	90.90%	84.80%
Median UMI Counts Per Cell	6726	6230

Clustering was performed as previously described (Nowakowski et al., 2017). Normalized counts matrices were $\log_2$ transformed, and variable genes were calculated using default Seurat parameters. Data were scaled in the space of these variable, and batch was regressed out. Principal component analysis was performed using FastPCA, and significant PCs were identified using the formula outlined in Shekhar et al. (2016). In the space of these significant PCs, the k=10 nearest neighbors were identified as per the RANN R package. The distances between these neighbors were weighted by their Jaccard distance, and louvain clustering was performed using the igraph R package. If any clusters contained only 1 cell, the process was repeated with k=11 and up until no clusters contained only 1 cell. Cluster markers and tSNE (t-Distributed Stochastic Neighbor Embedding) plots were generated with Seurat package default parameters. Differentially expressed genes for each cluster were shown in Figures S6 and S7.

Cell lineages trajectory was analyzed using Monocle 2, a computational method based on a machine learning technique called *reversed graph embedding* to construct the single-cell trajectories (Trapnell et al., 2014). Monocle uses the algorithm to extract the sequence of gene expression changes each cell must go through in biological processes, therefore, to predict lineage trajectories and bifurcations by ordering the pseudo-timeline. The pseudo-timeline is a developmental tree, that a cell at the beginning of the biological process starts at the root and progresses along the trunk and choose different path to finally arrive the leaf. A cell's pseudotime value is the distance that it would have to travel to get back to the root. The lineage trajectory reconstructed by monocle is referred to as predicted developmental trajectory. The cluster of RGC serves as the root point.

To analyze the events of lineage switch for cortical progenitors, we extracted the progenitor cells (including clusters of RGC, OB-IPC, OPC, and tri-IPC) from the Shh-IUE sample. We pooled all the subpopulations for the following analysis. We first imported the Seurat object containing cleaned, standardized, and clustered dataset to the monocle 2. Then, the most dispersed genes to use for pseudo-time ordering were calculated using the 'estimate dispersions' function. R package DDRTree was used to reduce dimensions with selected dispersed genes. In the meantime, the effects of numbers of UMI, donor, and library preparation batch were corrected. Finally, visualization function 'plot_cell_trajectory' was used to plot the minimum spanning tree on cells.

QUANTIFICATION AND STATISTICAL ANALYSIS

RNA-Seq data, scRNA-seq data and analysis are provided in the above methods sections. Statistical tests were performed using GraphPad Prism software, Microsoft Excel and R language. No statistical methods were used to estimate sample size. Number of cells are shown as mean ± SEM and statistical significance was determined using two-tailed Student's *t* tests. Significance was set as * for $p < 0.05$, ** for $p < 0.01$, and *** $p < 0.001$.

DATA AND CODE AVAILABILITY

Bulk RNA-seq data and scRNA-Seq data have been deposited at the National Center for Biotechnology Information BioProjects Gene Expression Omnibus and are accessible through GEO: GSE140817.

Supplementary Material

Refer to Web version on PubMed Central for supplementary material.

ACKNOWLEDGEMENTS

This study was supported by grants to Z.Y. from National Key Research and Development Program of China (2018YFA0108000), the National Natural Science Foundation of China (NSFC 31630032 and 31820103006), the Shanghai Municipal Science and Technology Major Project (2018SHZDZX01), and ZJLab; grants to B.C. from NIH (R01MH094589 and R01NS089777); a National Institutes of Health (NIH) grant to A.B. (K99 NS111731); a National Institute of Neurological Disorders and Stroke (NINDS) grant to A.R.K. (R35NS097305); and a National Institute of Mental Health (NIMH) grant to J.L.R. (MH049428). The authors thank Dr. Kazuaki Yoshikawa for providing the DLX2 antibody, Dr. Alexandra Joyner for providing *Gli2*$^{F/F}$ and *Gli3*$^{F/F}$ mice, and Drs. Sofie Salama (University of California, Santa Cruz [UCSC]), Josh Stuart (UCSC), Tom Nowakowski (University of California, San Francisco [UCSF]), and Alex Pollen (UCSF) for scientific discussions.

REFERENCES

Anderson SA, Eisenstat DD, Shi L, and Rubenstein JL (1997). Interneuron migration from basal forebrain to neocortex: dependence on Dlx genes. Science 278, 474–476. [PubMed: 9334308]

Balordi F, and Fishell G (2007). Hedgehog signaling in the subventricular zone is required for both the maintenance of stem cells and the migration of newborn neurons. J. Neurosci 27, 5936–5947. [PubMed: 17537964]

Bayraktar OA, Fuentealba LC, Alvarez-Buylla A, and Rowitch DH (2014). Astrocyte development and heterogeneity. Cold Spring Harb. Perspect. Biol 7, a020362. [PubMed: 25414368]

Blaess S, Stephen D, and Joyner AL (2008). Gli3 coordinates three-dimensional patterning and growth of the tectum and cerebellum by integrating Shh and Fgf8 signaling. Development 135, 2093–2103. [PubMed: 18480159]

Blondel VD, Guillaume J-L, Lambiotte R, and Lefebvre E (2008). Fast unfolding of communities in large networks. J. Stat. Mech 10, P10008.

Buchholz F, Angrand PO, and Stewart AF (1998). Improved properties of FLP recombinase evolved by cycling mutagenesis. Nat. Biotechnol 16, 657–662. [PubMed: 9661200]

Bulfone A, Martinez S, Marigo V, Campanella M, Basile A, Quaderi N, Gattuso C, Rubenstein JL, and Ballabio A (1999). Expression pattern of the Tbr2 (Eomesodermin) gene during mouse and chick brain development. Mech. Dev 84, 133–138. [PubMed: 10473127]

Cai Y, Zhang Y, Shen Q, Rubenstein JL, and Yang Z (2013). A subpopulation of individual neural progenitors in the mammalian dorsal pallium generates both projection neurons and interneurons in vitro. Stem Cells 31, 1193–1201. [PubMed: 23417928]

Chapman H, Waclaw RR, Pei Z, Nakafuku M, and Campbell K (2013). The homeobox gene Gsx2 controls the timing of oligodendroglial fate specification in mouse lateral ganglionic eminence progenitors. Development 140, 2289–2298. [PubMed: 23637331]

Chapman H, Riesenberg A, Ehrman LA, Kohli V, Nardini D, Nakafuku M, Campbell K, and Waclaw RR (2018). Gsx transcription factors control neuronal versus glial specification in ventricular zone progenitors of the mouse lateral ganglionic eminence. Dev. Biol 442, 115–126. [PubMed: 29990475]

Corrales JD, Blaess S, Mahoney EM, and Joyner AL (2006). The level of sonic hedgehog signaling regulates the complexity of cerebellar foliation. Development 133, 1811–1821. [PubMed: 16571625]

Desmaris E, Keruzore M, Saulnier A, Ratié L, Assimacopoulos S, De Clercq S, Nan X, Roychoudhury K, Qin S, Kricha S, et al. (2018). DMRT5, DMRT3, and EMX2 cooperatively repress *Gsx2* at the pallium-subpallium boundary to maintain cortical identity in dorsal telencephalic progenitors. J. Neurosci 38, 9105–9121. [PubMed: 30143575]

Doe CQ (2017). Temporal patterning in the *Drosophila* CNS. Annu. Rev. Cell Dev. Biol 33, 219–240. [PubMed: 28992439]

Englund C, Fink A, Lau C, Pham D, Daza RA, Bulfone A, Kowalczyk T, and Hevner RF (2005). Pax6, Tbr2, and Tbr1 are expressed sequentially by radial glia, intermediate progenitor cells, and postmitotic neurons in developing neocortex. J. Neurosci 25, 247–251. [PubMed: 15634788]

Fuentealba LC, Rompani SB, Parraguez JI, Obernier K, Romero R, Cepko CL, and Alvarez-Buylla A (2015). Embryonic Origin of Postnatal Neural Stem Cells. Cell 161, 1644–1655. [PubMed: 26091041]

Gao P, Postiglione MP, Krieger TG, Hernandez L, Wang C, Han Z, Streicher C, Papusheva E, Insolera R, Chugh K, et al. (2014). Deterministic progenitor behavior and unitary production of neurons in the neocortex. Cell 159, 775–788. [PubMed: 25417155]

Gorski JA, Talley T, Qiu M, Puelles L, Rubenstein JL, and Jones KR (2002). Cortical excitatory neurons and glia, but not GABAergic neurons, are produced in the Emx1-expressing lineage. J. Neurosci 22, 6309–6314. [PubMed: 12151506]

Guo C, Eckler MJ, McKenna WL, McKinsey GL, Rubenstein JL, and Chen B (2013). Fezf2 expression identifies a multipotent progenitor for neocortical projection neurons, astrocytes, and oligodendrocytes. Neuron 80, 1167–1174. [PubMed: 24314728]

Guo T, Liu G, Du H, Wen Y, Wei S, Li Z, Tao G, Shang Z, Song X, Zhang Z, et al. (2019). Dlx1/2 are Central and Essential Components in the Transcriptional Code for Generating Olfactory Bulb Interneurons. Cereb. Cortex 29, 4831–4849. [PubMed: 30796806]

Hasenpusch-Theil K, Magnani D, Amaniti EM, Han L, Armstrong D, and Theil T (2012). Transcriptional analysis of Gli3 mutants identifies Wnt target genes in the developing hippocampus. Cereb. Cortex 22, 2878–2893. [PubMed: 22235033]

Hasenpusch-Theil K, West S, Kelman A, Kozic Z, Horrocks S, McMahon AP, Price DJ, Mason JO, and Theil T (2018). Gli3 controls the onset of cortical neurogenesis by regulating the radial glial cell cycle through *Cdk6* expression. Development 145, dev163147. [PubMed: 30093555]

He M, Tucciarone J, Lee S, Nigro MJ, Kim Y, Levine JM, Kelly SM, Krugikov I, Wu P, Chen Y, et al. (2016). Strategies and Tools for combinatorial targeting of GABAergic neurons in mouse cerebral cortex. Neuron 91, 1228–1243. [PubMed: 27618674]

Hébert JM, and Fishell G (2008). The genetics of early telencephalon patterning: some assembly required. Nat. Rev. Neurosci 9, 678–685. [PubMed: 19143049]

Hevner RF (2019). Intermediate progenitors and Tbr2 in cortical development. J. Anat 235, 616–625. [PubMed: 30677129]

Hu JS, Vogt D, Sandberg M, and Rubenstein JL (2017). Cortical interneuron development: a tale of time and space. Development 144, 3867–3878. [PubMed: 29089360]

Hui CC, and Angers S (2011). Gli proteins in development and disease. Annu. Rev. Cell Dev. Biol 27, 513–537. [PubMed: 21801010]

Jeong J, Mao J, Tenzen T, Kottmann AH, and McMahon AP (2004). Hedgehog signaling in the neural crest cells regulates the patterning and growth of facial primordia. Genes Dev. 18, 937–951. [PubMed: 15107405]

Kessaris N, Fogarty M, Iannarelli P, Grist M, Wegner M, and Richardson WD (2006). Competing waves of oligodendrocytes in the forebrain and postnatal elimination of an embryonic lineage. Nat. Neurosci 9, 173–179. [PubMed: 16388308]

Kohwi M, and Doe CQ (2013). Temporal fate specification and neural progenitor competence during development. Nat. Rev. Neurosci 14, 823–838. [PubMed: 24400340]

Kohwi M, Petryniak MA, Long JE, Ekker M, Obata K, Yanagawa Y, Rubenstein JL, and Alvarez-Buylla A (2007). A subpopulation of olfactory bulb GABAergic interneurons is derived from Emx1- and Dlx5/6-expressing progenitors. J. Neurosci 27, 6878–6891. [PubMed: 17596436]

Komada M, Iguchi T, Takeda T, Ishibashi M, and Sato M (2013). Smoothened controls cyclin D2 expression and regulates the generation of intermediate progenitors in the developing cortex. Neurosci. Lett 547, 87–91. [PubMed: 23680462]

Kowalczyk T, Pontious A, Englund C, Daza RA, Bedogni F, Hodge R, Attardo A, Bell C, Huttner WB, and Hevner RF (2009). Intermediate neuronal progenitors (basal progenitors) produce pyramidal-projection neurons for all layers of cerebral cortex. Cereb. Cortex 19, 2439–2450. [PubMed: 19168665]

Kriegstein A, and Alvarez-Buylla A (2009). The glial nature of embryonic and adult neural stem cells. Annu. Rev. Neurosci 32, 149–184. [PubMed: 19555289]

Kuwajima T, Nishimura I, and Yoshikawa K (2006). Necdin promotes GABAergic neuron differentiation in cooperation with Dlx homeodomain proteins. J. Neurosci 26, 5383–5392. [PubMed: 16707790]

Kwan KY, Sestan N, and Anton ES (2012). Transcriptional co-regulation of neuronal migration and laminar identity in the neocortex. Development 139, 1535–1546. [PubMed: 22492350]

Leone DP, Srinivasan K, Chen B, Alcamo E, and McConnell SK (2008). The determination of projection neuron identity in the developing cerebral cortex. Curr. Opin. Neurobiol 18, 28–35. [PubMed: 18508260]

Li J, Wang C, Zhang Z, Wen Y, An L, Liang Q, Xu Z, Wei S, Li W, Guo T, et al. (2018). Transcription Factors Sp8 and Sp9 Coordinately Regulate Olfactory Bulb Interneuron Development. Cereb. Cortex 28, 3278–3294. [PubMed: 28981617]

Lim L, Mi D, Llorca A, and Marín O (2018). Development and Functional Diversification of Cortical Interneurons. Neuron 100, 294–313. [PubMed: 30359598]

Lindtner S, Catta-Preta R, Tian H, Su-Feher L, Price JD, Dickel DE, Greiner V, Silberberg SN, McKinsey GL, McManus MT, et al. (2019). Genomic resolution of DLX-orchestrated transcriptional circuits driving development of forebrain GABAergic neurons. Cell Rep. 28, 2048–2063.e8. [PubMed: 31433982]

Liu Z, Zhang Z, Lindtner S, Li Z, Xu Z, Wei S, Liang Q, Wen Y, Tao G, You Y, et al. (2019). Sp9 regulates medial ganglionic eminence-derived cortical interneuron development. Cereb. Cortex 29, 2653–2667. [PubMed: 29878134]

Long JE, Garel S, Alvarez-Dolado M, Yoshikawa K, Osumi N, Alvarez-Buylla A, and Rubenstein JL (2007). Dlx-dependent and -independent regulation of olfactory bulb interneuron differentiation. J. Neurosci 27, 3230–3243. [PubMed: 17376983]

Lv X, Ren SQ, Zhang XJ, Shen Z, Ghosh T, Xianyu A, Gao P, Li Z, Lin S, Yu Y, et al. (2019). TBR2 coordinates neurogenesis expansion and precise microcircuit organization via Protocadherin 19 in the mammalian cortex. Nat. Commun 10, 3946. [PubMed: 31477701]

Ma T, Zhang Q, Cai Y, You Y, Rubenstein JL, and Yang Z (2012). A subpopulation of dorsal lateral/caudal ganglionic eminence-derived neocortical interneurons expresses the transcription factor Sp8. Cereb. Cortex 22, 2120–2130. [PubMed: 22021915]

Macosko EZ, Basu A, Satija R, Nemesh J, Shekhar K, Goldman M, Tirosh I, Bialas AR, Kamitaki N, Martersteck EM, et al. (2015). Highly parallel genome-wide expression profiling of individual cells using nanoliter droplets. Cell 161, 1202–1214. [PubMed: 26000488]

Merkle FT, Mirzadeh Z, and Alvarez-Buylla A (2007). Mosaic organization of neural stem cells in the adult brain. Science 317, 381–384. [PubMed: 17615304]

Mihalas AB, Elsen GE, Bedogni F, Daza RAM, Ramos-Laguna KA, Arnold SJ, and Hevner RF (2016). Intermediate progenitor cohorts differentially generate cortical layers and require Tbr2 for timely acquisition of neuronal subtype identity. Cell Rep. 16, 92–105. [PubMed: 27320921]

Noctor SC, Martínez-Cerdeño V, Ivic L, and Kriegstein AR (2004). Cortical neurons arise in symmetric and asymmetric division zones and migrate through specific phases. Nat. Neurosci 7, 136–144. [PubMed: 14703572]

Nowakowski TJ, Bhaduri A, Pollen AA, Alvarado B, Mostajo-Radji MA, Di Lullo E, Haeussler M, Sandoval-Espinosa C, Liu SJ, Velmeshev D, et al. (2017). Spatiotemporal gene expression trajectories reveal developmental hierarchies of the human cortex. Science 358, 1318–1323. [PubMed: 29217575]

Obernier K, and Alvarez-Buylla A (2019). Neural stem cells: origin, heterogeneity and regulation in the adult mammalian brain. Development 146, dev156059. [PubMed: 30777863]

Ohkubo Y, Chiang C, and Rubenstein JL (2002). Coordinate regulation and synergistic actions of BMP4, SHH and FGF8 in the rostral prosencephalon regulate morphogenesis of the telencephalic and optic vesicles. Neuroscience 111, 1–17. [PubMed: 11955708]

Petrova R, Garcia AD, and Joyner AL (2013). Titration of GLI3 repressor activity by sonic hedgehog signaling is critical for maintaining multiple adult neural stem cell and astrocyte functions. J. Neurosci 33, 17490–17505. [PubMed: 24174682]

Petryniak MA, Potter GB, Rowitch DH, and Rubenstein JL (2007). Dlx1 and Dlx2 control neuronal versus oligodendroglial cell fate acquisition in the developing forebrain. Neuron 55, 417–433. [PubMed: 17678855]

Potter GB, Petryniak MA, Shevchenko E, McKinsey GL, Ekker M, and Rubenstein JL (2009). Generation of Cre-transgenic mice using Dlx1/Dlx2 enhancers and their characterization in GABAergic interneurons. Mol. Cell. Neurosci 40, 167–186. [PubMed: 19026749]

Qiu X, Hill A, Packer J, Lin D, Ma YA, and Trapnell C (2017a). Single-cell mRNA quantification and differential analysis with Census. Nat. Methods 14, 309–315. [PubMed: 28114287]

Qiu X, Mao Q, Tang Y, Wang L, Chawla R, Pliner HA, and Trapnell C (2017b). Reversed graph embedding resolves complex single-cell trajectories. Nat. Methods 14, 979–982. [PubMed: 28825705]

Raff MC, Miller RH, and Noble M (1983). A glial progenitor cell that develops in vitro into an astrocyte or an oligodendrocyte depending on culture medium. Nature 303, 390–396. [PubMed: 6304520]

Rallu M, Machold R, Gaiano N, Corbin JG, McMahon AP, and Fishell G (2002). Dorsoventral patterning is established in the telencephalon of mutants lacking both Gli3 and Hedgehog signaling. Development 129, 4963–4974. [PubMed: 12397105]

Shekhar K, Lapan SW, Whitney IE, Tran NM, Macosko EZ, Kowalczyk M, Adiconis X, Levin JZ, Nemesh J, Goldman M, et al. (2016). Comprehensive classification of retinal bipolar neurons by single-cell transcriptomics. Cell 166, 1308–1323.e30. [PubMed: 27565351]

Shikata Y, Okada T, Hashimoto M, Ellis T, Matsumaru D, Shiroishi T, Ogawa M, Wainwright B, and Motoyama J (2011). Ptch1-mediated dosage-dependent action of Shh signaling regulates neural progenitor development at late gestational stages. Dev. Biol 349, 147–159. [PubMed: 20969845]

Sousa VH, and Fishell G (2010). Sonic hedgehog functions through dynamic changes in temporal competence in the developing forebrain. Curr. Opin. Genet. Dev 20, 391–399. [PubMed: 20466536]

Stenman J, Toresson H, and Campbell K (2003). Identification of two distinct progenitor populations in the lateral ganglionic eminence: implications for striatal and olfactory bulb neurogenesis. J. Neurosci 23, 167–174. [PubMed: 12514213]

Theil T, Alvarez-Bolado G, Walter A, and Rüther U (1999). Gli3 is required for Emx gene expression during dorsal telencephalon development. Development 126, 3561–3571. [PubMed: 10409502]

Tole S, Ragsdale CW, and Grove EA (2000). Dorsoventral patterning of the telencephalon is disrupted in the mouse mutant extra-toes(J). Dev. Biol 217, 254–265. [PubMed: 10625551]

Tong CK, Fuentealba LC, Shah JK, Lindquist RA, Ihrie RA, Guinto CD, Rodas-Rodriguez JL, and Alvarez-Buylla A (2015). A dorsal SHH-dependent domain in the V-SVZ produces large numbers of oligodendroglial lineage cells in the postnatal brain. Stem Cell Reports 5, 461–470. [PubMed: 26411905]

Toresson H, and Campbell K (2001). A role for Gsh1 in the developing striatum and olfactory bulb of Gsh2 mutant mice. Development 128, 4769–4780. [PubMed: 11731457]

Trapnell C, Roberts A, Goff L, Pertea G, Kim D, Kelley DR, Pimentel H, Salzberg SL, Rinn JL, and Pachter L (2012). Differential gene and transcript expression analysis of RNA-seq experiments with TopHat and Cufflinks. Nat. Protoc 7, 562–578. [PubMed: 22383036]

Trapnell C, Cacchiarelli D, Grimsby J, Pokharel P, Li S, Morse M, Lennon NJ, Livak KJ, Mikkelsen TS, and Rinn JL (2014). The dynamics and regulators of cell fate decisions are revealed by pseudotemporal ordering of single cells. Nat. Biotechnol 32, 381–386. [PubMed: 24658644]

Vasistha NA, García-Moreno F, Arora S, Cheung AF, Arnold SJ, Robertson EJ, and Molnár Z (2015). Cortical and clonal contribution of Tbr2 expressing progenitors in the developing mouse brain. Cereb. Cortex 25, 3290–3302. [PubMed: 24927931]

Ventura RE, and Goldman JE (2007). Dorsal radial glia generate olfactory bulb interneurons in the postnatal murine brain. J. Neurosci 27, 4297–4302. [PubMed: 17442813]

Waclaw RR, Wang B, Pei Z, Ehrman LA, and Campbell K (2009). Distinct temporal requirements for the homeobox gene Gsx2 in specifying striatal and olfactory bulb neuronal fates. Neuron 63, 451–465. [PubMed: 19709628]

Wang B, Waclaw RR, Allen ZJ 2nd, Guillemot F, and Campbell K (2009). Ascl1 is a required downstream effector of Gsx gene function in the embryonic mouse telencephalon. Neural Dev. 4, 5. [PubMed: 19208224]

Wang B, Long JE, Flandin P, Pla R, Waclaw RR, Campbell K, and Rubenstein JL (2013). Loss of Gsx1 and Gsx2 function rescues distinct pheno-types in Dlx1/2 mutants. J. Comp. Neurol 521, 1561–1584. [PubMed: 23042297]

Wang H, Kane AW, Lee C, and Ahn S (2014). Gli3 repressor controls cell fates and cell adhesion for proper establishment of neurogenic niche. Cell Rep. 8, 1093–1104. [PubMed: 25127137]

Wen Y, Zhang Z, Li Z, Liu G, Tao G, Song X, Xu Z, Shang Z, Guo T, Su Z, et al. (2019). The PROK2/PROKR2 signaling pathway is required for the migration of most olfactory bulb interneurons. J. Comp. Neurol 527, 2931–2947. [PubMed: 31132148]

Winkler CC, and Franco SJ (2019). Loss of Shh signaling in the neocortex reveals heterogeneous cell recovery responses from distinct oligodendrocyte populations. Dev. Biol 452, 55–65. [PubMed: 31071314]

Winkler CC, Yabut OR, Fregoso SP, Gomez HG, Dwyer BE, Pleasure SJ, and Franco SJ (2018). The dorsal wave of neocortical oligodendrogenesis begins embryonically and requires multiple sources of sonic hedgehog. J. Neurosci 38, 5237–5250. [PubMed: 29739868]

Yabut OR, Fernandez G, Huynh T, Yoon K, and Pleasure SJ (2015). Suppressor of fused is critical for maintenance of neuronal progenitor identity during corticogenesis. Cell Rep. 12, 2021–2034. [PubMed: 26387942]

Young KM, Fogarty M, Kessaris N, and Richardson WD (2007). Subventricular zone stem cells are heterogeneous with respect to their embryonic origins and neurogenic fates in the adult olfactory bulb. J. Neurosci 27, 8286–8296. [PubMed: 17670975]

Zhang Q, Zhang Y, Wang C, Xu Z, Liang Q, An L, Li J, Liu Z, You Y, He M, et al. (2016). The zinc finger transcription factor Sp9 is required for the development of striatopallidal projection neurons. Cell Rep. 16, 1431–1444. [PubMed: 27452460]

Zhuo L, Theis M, Alvarez-Maya I, Brenner M, Willecke K, and Messing A (2001). hGFAP-cre transgenic mice for manipulation of glial and neuronal function in vivo. Genesis 31, 85–94. [PubMed: 11668683]

Highlights

- Cortical NSC-derived $GSX2^+$ IPC population has tri-potential
- SHH signaling is crucial for cortical NSCs to generate OB interneurons
- SHH regulates OB interneuron and cortical glia production by reducing GLI3R
- scRNA-seq analysis identifies molecular signatures of $GSX2^+$ IPCs in the cortex

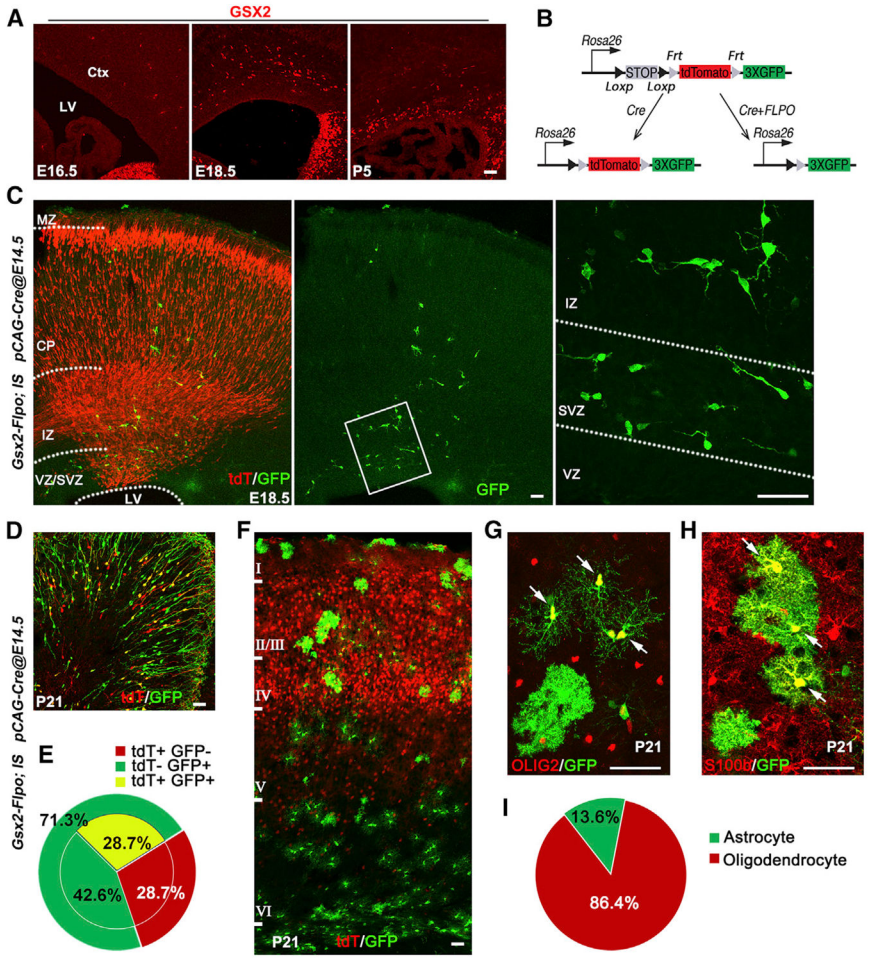

Figure 1. Cortical NSCs Generate GSX2^{+} Tri-IPCs That Give Rise Not Only to OB Interneurons but Also to Cortical Oligodendrocytes and Astrocytes

(A) GSX2^{+} IPCs in the mouse cortical SVZ at E16.5, E18.5, and P5. Ctx, cortex; LV, lateral ventricle.

(B) The strategy of the intersectional lineage analysis.

(C) Plasmids *pCAG-Cre* were electroporated to the cortical VZ of *Gsx2$^{Flpo/+}$; IS* mice at E14.5. GFP^{+} cells were observed in the SVZ and cortical plate at E18.5. CP, cortical plate; IZ, intermediate zone; MZ, marginal zone.

(D) GFP^{+} and/or tdT^{+} interneurons in the OB at P21.

(E) Quantification of the percentages of GFP^{+} and tdT^{+} cells among all the lineage-traced cells in the OB.

(F–H) Cortical GFP^{+} oligodendrocytes (OLIG2^{+}, arrows in G) and astrocytes (S100b^{+}, arrows in H) with higher magnification images at P21. Note tdT^{+} PyNs located in cortical layers II–V (F).

(I) Percentages of oligodendrocytes and astrocytes among all GFP^{+} cells in the cortex.

Data in (E) and (I) were from three mice each. Scale bars, 50 mm in (A), (C), (D), and (F)–(H).

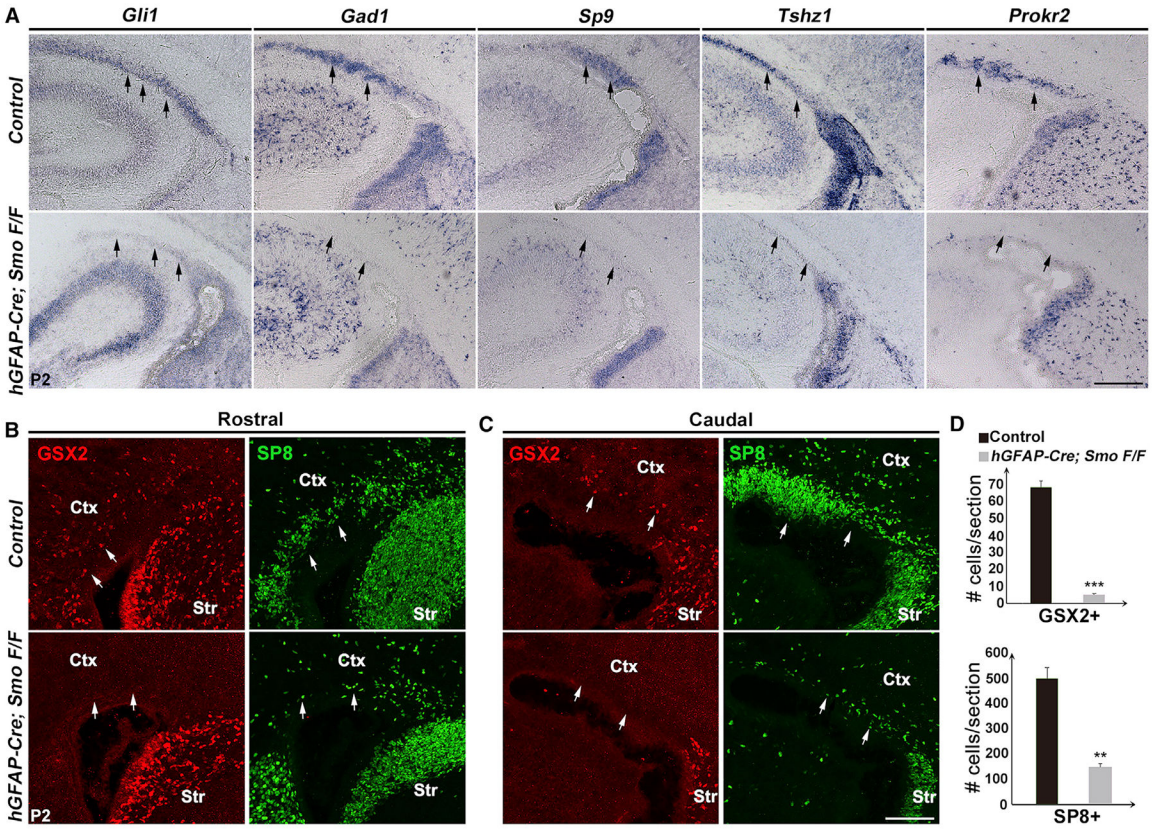

Figure 2. Cells of the OB Interneuron Lineage Are Not Generated in the Cortical SVZ of Smo cko Mice at P2

(A) *In situ* RNA hybridization showing expressions of *Gli1*, *Gad1*, *Sp9*, *Tshz1*, and *Prokr2* in the caudal cortical SVZ (arrows) in the control and *hGFAP-Cre; Smo*$^{F/F}$ (*Smo cko*) mice.

(B and C) GSX2 and SP8 (arrows) immunostainings of the rostral (B) and caudal (C) cortical sections from control and *Smo cko* mice at P2. Ctx, cortex; Str, striatum.

(D) Numbers of GSX2^{+} and SP8^{+} cells in the cortical SVZ per section.

Data are presented as means ± SEM; n = 3. ***p < 0.001, **p < 0.01; Student's t test. Scale bars, 200 mm in (B) and (D).

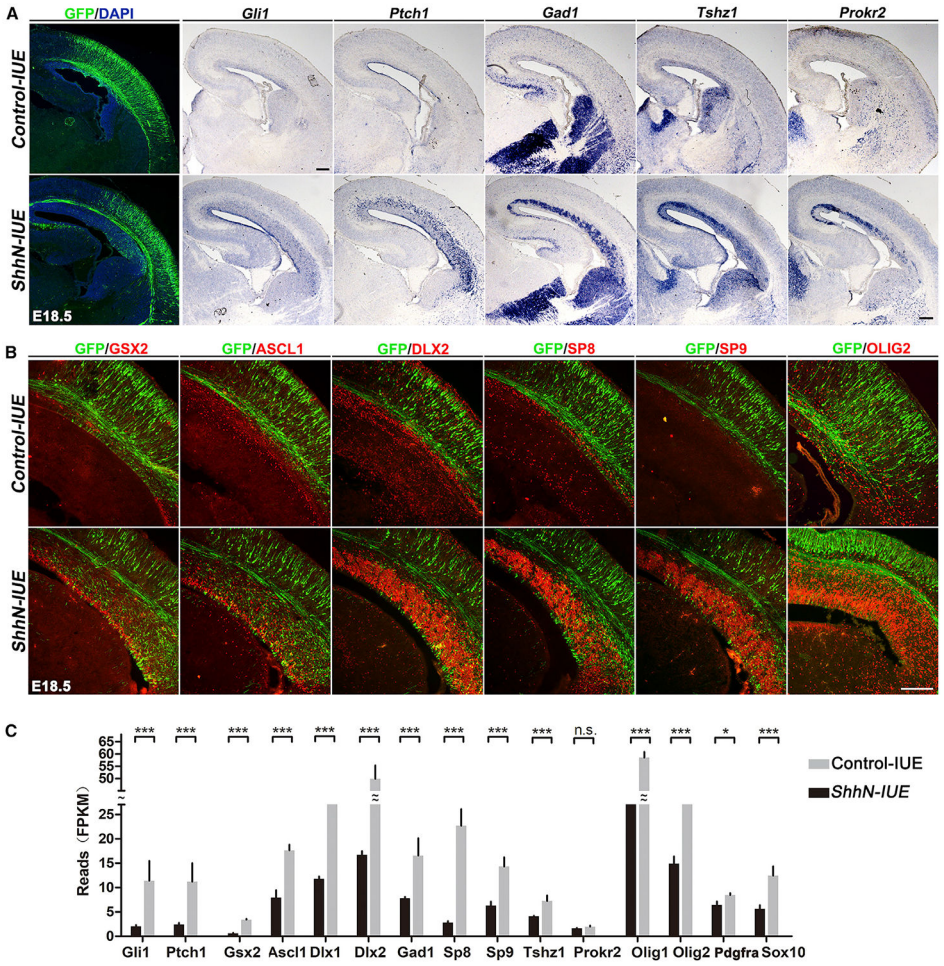

Figure 3. Overexpression of ShhN in the Cortex by IUE Induces OB Interneuron and Oligodendrocyte Lineages in the Cortical SVZ

(A) Control *pCAG-GFP* plasmids (control-IUE) or *pCAG-ShhN-ires-GFP* plasmids (ShhN-IUE) were electroporated into the cortical VZ on E13.5. The E18.5 brains were analyzed. The distribution patterns of electroporated cells (GFP^+) in the cortex are shown. Note that the mRNA levels of *Gli1*, *Ptch1*, *Gad1*, *Tshz1*, and *Prokr2* were dramatically increased in the *ShhN-IUE* cortex.

(B) The expressions of GSX2, ASCL1, DLX2, SP8, SP9, and OLIG2 were greatly increased in the *ShhN*-IUE cortex.

(C) RNA-seq analysis revealed increased expression levels for SHH pathway target genes, OB interneuron lineage and oligodendrocyte lineage genes in the *ShhN-IUE* cortices at P0. Data are presented as means ± SEM; n = 3. ***p < 0.001, *p < 0.05; n.s., non-significant; Student's t test in (C). Scale bars, 200 mm in (A) and (B).

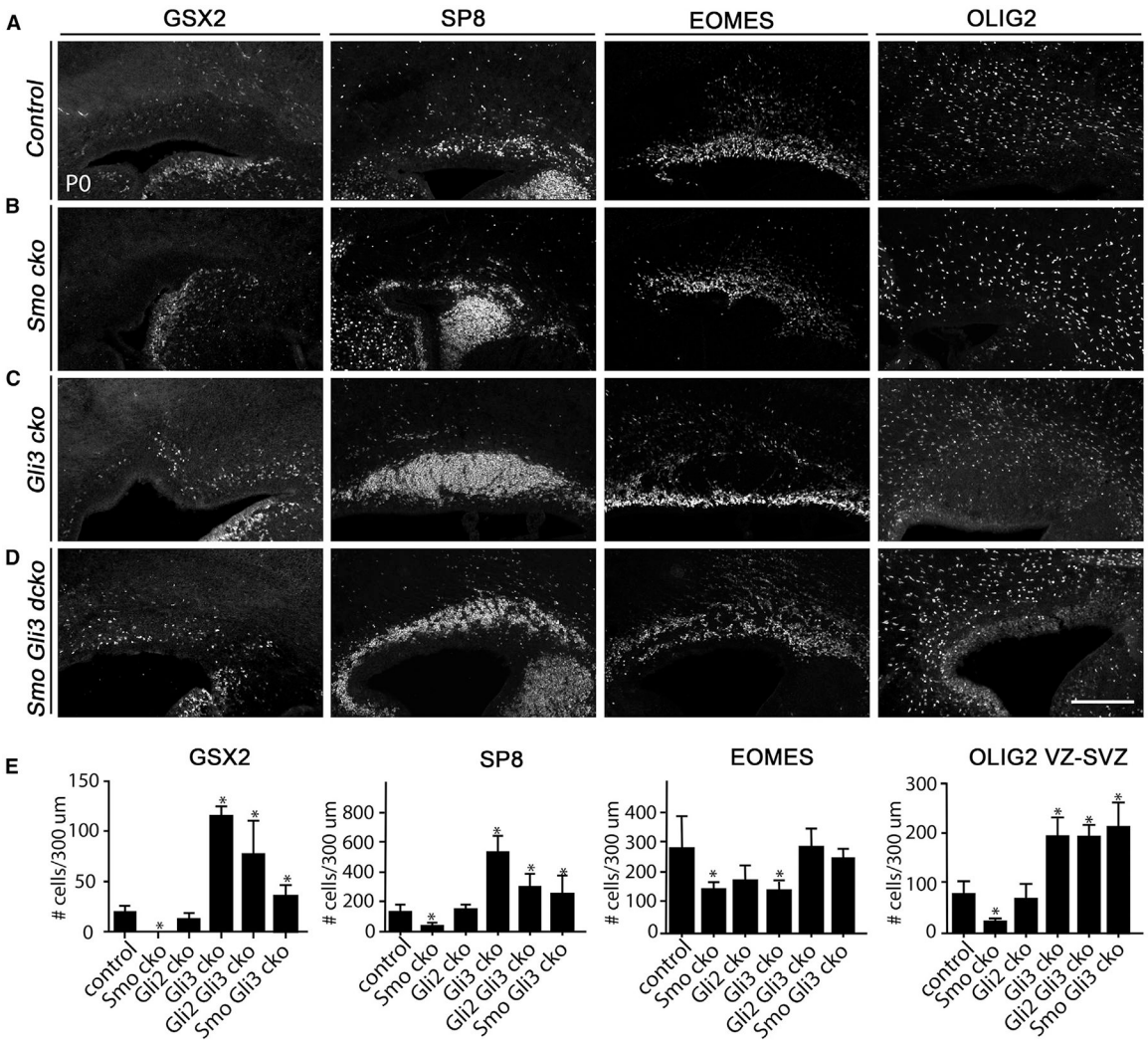

Figure 4. SHH Regulates the Production of OB Interneurons and Oligodendrocytes in the Cortical SVZ Predominately by Reducing GLI3

(A–D) Immunostainings for GSX2, SP8, EOMES, and OLIG2 in wild-type (control) (A), *Smo cko* (B), *Gli3 cko* (C), and *Smo Gli3 dcko* (D) mice at P0.

(E) Quantification for the numbers of $GSX2^+$, $SP8^+$, $EOMES^+$, and $OLIG2^+$ cells per 300 mm width in the cortical VZ-SVZ of control and mutant mice at P0. Data are presented as means ± SEM; n = 3 mice per genotype. *$p < 0.05$; unpaired Student's t test in (E). Scale bars, 200 mm in (D).

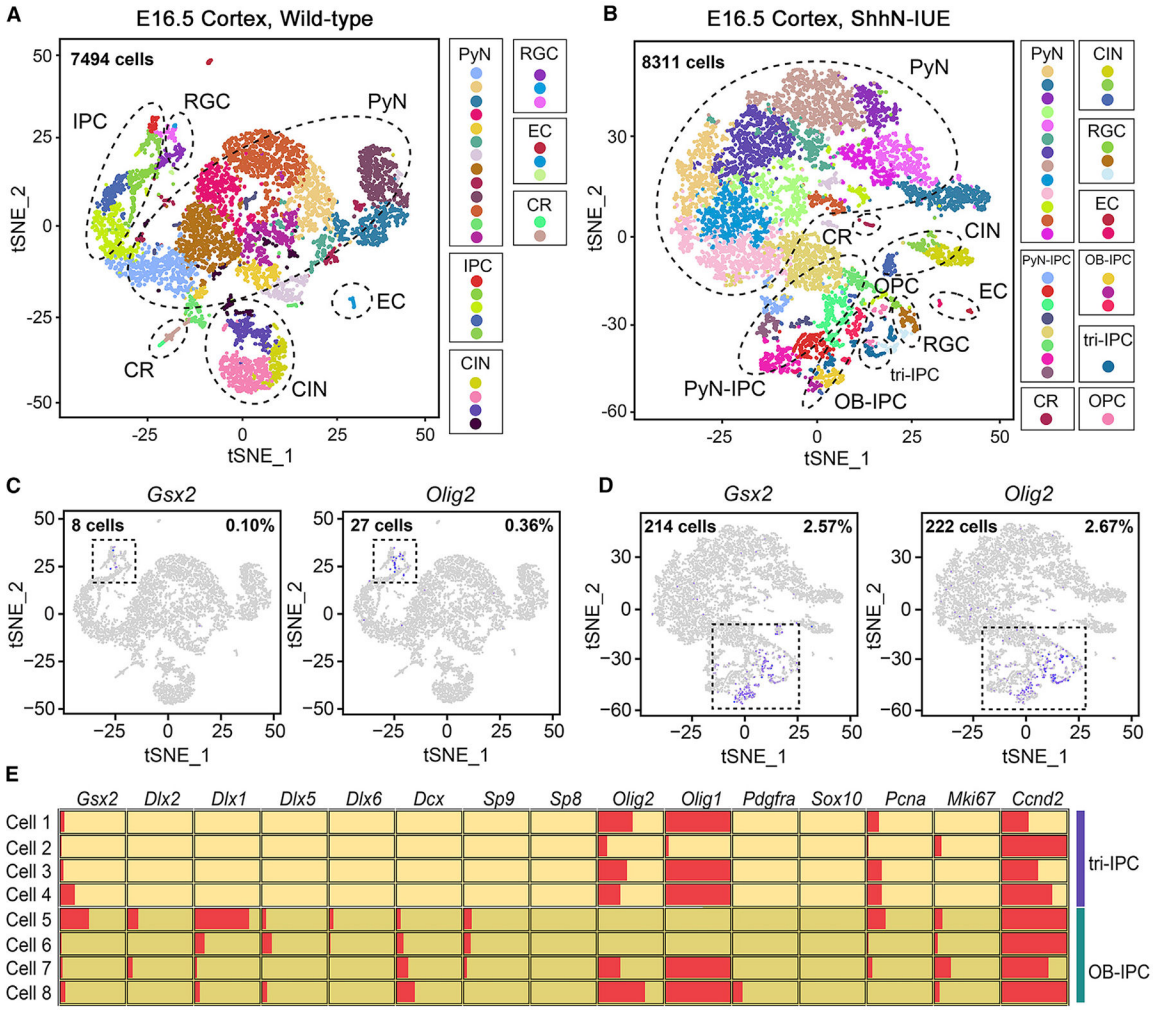

Figure 5. scRNA-Seq Analysis of Cells in the E16.5 Wild-Type Cortices and in the ShhN-IUE Cortices

(A and B) Scatterplot of cells after principal-component analysis and t-SNE visualization, colored according to Seurat clustering and annotated by major cell types for all the cells in the wild-type sample (A) and the *ShhN*-IUE sample (B).

(C and D) t-SNE of cells colored by mean expression of *Gsx2* and *Olig2* in wild-type (C) and *ShhN*-IUE (D) samples.

(E) The eight *Gsx2*$^{+}$ cells in the E16.5 wild-type sample consisted of four tri-IPCs and four OB-IPCs, based on the expressions of specific genes.

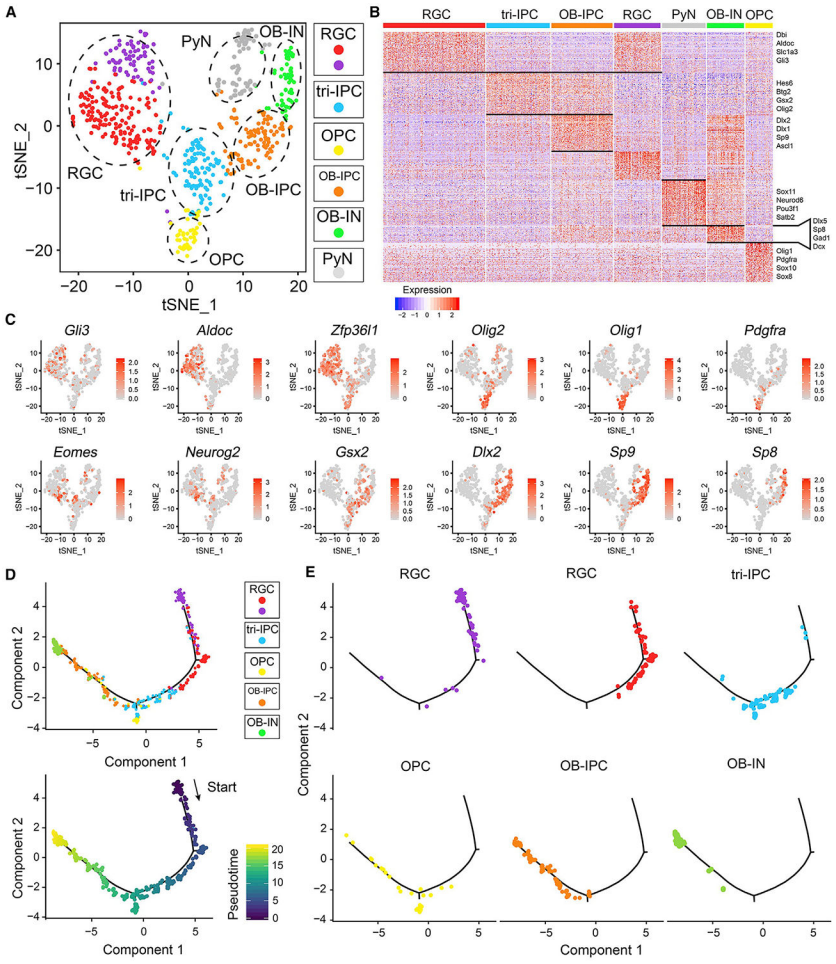

Figure 6. scRNA-Seq Analysis of the Progenitor Cells in the ShhN-IUE Sample

(A) Seurat clustering was performed on all the progenitor cells in the ShhN-IUE sample. Seven clusters were identified and annotated to six cell types based on gene expression features.

(B) Heatmap showing marker gene expressions in the seven cell clusters. Each column represents expressions in one cell, and each row represents expressions of one gene.

(C) The t-SNE plots of cells colored by mean expression of specific marker genes.

(D) Monocle analysis of all the progenitors in the ShhN-IUE samples revealed differentiation trajectories and pseudo-timelines along the cell differentiation axis. Each point represents a cell, colored by cluster identity (top) or pseudo-timeline (bottom).

(E) Seurat clusters shown along the predicted pseudo-timeline differentiation trajectory.

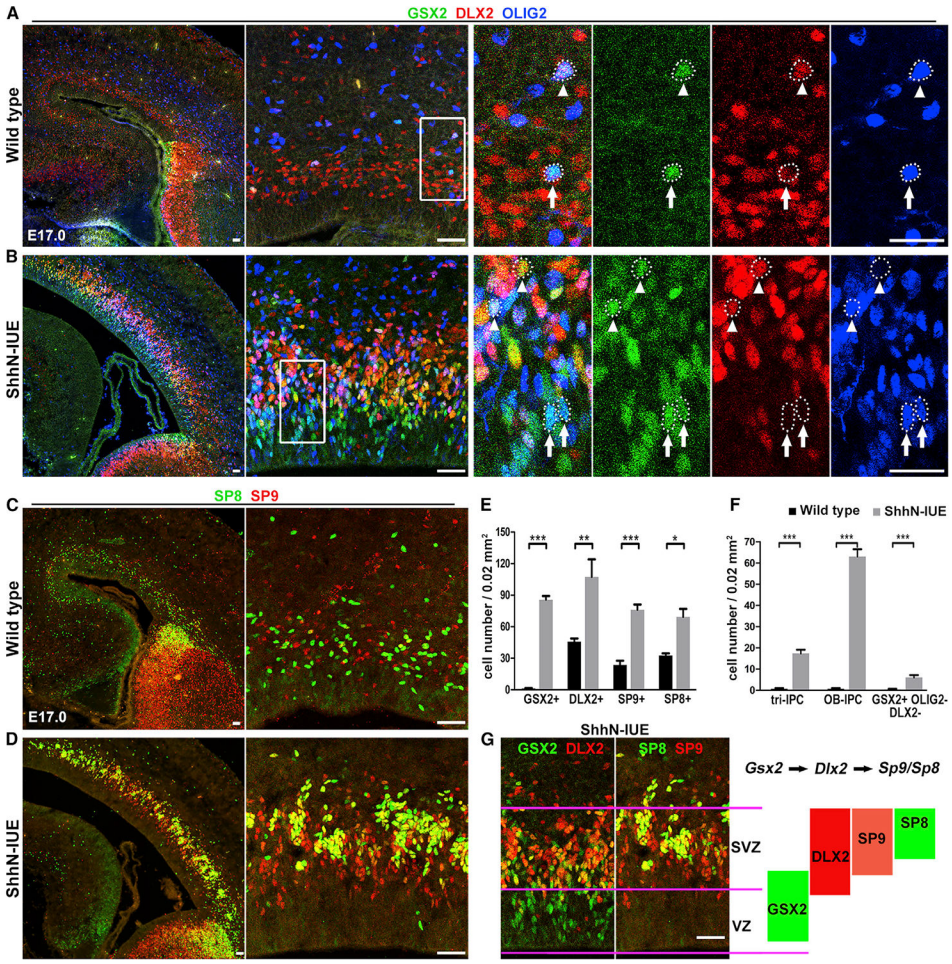

Figure 7. In Vivo Validation of Markers of Tri-IPCs and OB-IPCs

(A and B) The expression of GSX2, OLIG2, and DLX2 in the cortical VZ/SVZ of wild-type (A) and *ShhN-IUE* (B) mice at E17. Note that very few $GSX2^+$ cells (green) were present in the cortical SVZ. Arrows indicate $GSX2^+OLIG2^+DLX2$ tri-IPCs, and arrowheads indicate $GSX2^+DLX2^+$ OB-IPCs.

(C and D) The expression of SP9 and SP8 in the cortical VZ/SVZ of wild-type (C) and *ShhN-IUE* (D) mice at E17.

(E and F) More OB interneuron lineage cells (E) and more tri-IPCs and OB-IPCs (F) were observed in the *ShhN-IUE* cortices than in the controls.

(G) The sequential expression of GSX2/DLX2/SP9/SP8 is linked to lineage differentiation from tri-IPCs/OB-IPCs/OB neuroblasts, indicating the core transcriptional network for OB interneuron generation.

Data are presented as means ± SEM; n = 3 mice for each condition. ***$p < 0.001$, **$p < 0.01$, *$p < 0.05$; Student's t test in (E) and (F). Scale bars, 50 mm in (A)–(D) and (G).

KEY RESOURCES TABLE

REAGENT or RESOURCE	SOURCE	IDENTIFIER
Primary Antibodies		
Rabbit anti-GSX2	Millipore	Cat# ABN162; RRID: AB_11203296
Chicken anti-GFP	Aves Labs	Cat# GFP-1020; RRID: AB_2307313
Goat anti-tdTomato	SICGEN	Cat# AB8181; RRID: AB_2722750
Rabbit anti-OLIG2	Millipore	Cat# AB9610; RRID: AB_570666
Mouse anti-OLIG2	Millipore	Cat# MABN50; RRID: AB_10807410
Goat anti-SP8	Santa Cruz Biotechnology	Cat# sc-104661; RRID: AB_2194626
Rabbit anti-GFAP	Dako	Cat# Z0334; RRID: AB_10013382
Rabbit anti-S100	Dako	Cat# Z0311; RRID: AB_10013383
Rabbit anti-ASCL1	Cosmo Bio	Cat# SK-T01-003; RRID: AB_10709354
Guinea pig anti-DLX2	Guo et al., 2019; Kuwajima et al., 2006	
Mouse anti-MKI67	BD Pharmingen	Cat# 556003; RRID: AB_396287
Rabbit anti-SP9	(Zhang et al., 2016) Available from authors	
Rat anti-EOMES	Thermo Fisher	Cat# 12-4875-82; RRID: AB_1603275
Secondary antibodies		
Alexa Fluor®488 Donkey anti-Rabbit	Jackson ImmunoResearch	Cat# 711-546-152; RRID: AB_2340619
Cyanine Cy3 Donkey anti-Rabbit	Jackson ImmunoResearch	Cat# 711-166-152; RRID: AB_2313568
Alexa Fluor®488 Donkey anti-Goat	Jackson ImmunoResearch	Cat# 705-546-147; RRID: AB_2340430
Cyanine Cy3 Donkey anti-Goat	Jackson ImmunoResearch	Cat# 705-166-147; RRID: AB_2340413
Alexa Fluor®488 Donkey anti-Chicken	Jackson ImmunoResearch	Cat# 703-546-155; RRID: AB_2340376
Cyanine Cy3 Donkey anti-Guinea pig	Jackson ImmunoResearch	Cat# 706-166-148; RRID: AB_2340461
Alexa Fluor®488 Donkey anti-Rat	Jackson ImmunoResearch	Cat# 712-546-153; RRID: AB_2340686
Alexa Fluor®647 Donkey anti-Mouse	Jackson ImmunoResearch	Cat# 715-606-151; RRID: AB_2340866
Biological Samples		
Mouse cortex	This study	N/A
Deposited Data		
Raw and processed data	This study	GEO: GSE140817
Experimental Models: Strains/Organisms		
Gsx2^{Flpo}	This Study	N/A
Rosa26-tdTomato-FRT	He et al., 2016	N/A
IS reporter	The Jackson Laboratory	Stock No. 028582
Emx1$^{Cre/+}$	The Jackson Laboratory	Stock No. 005628
Smo^{FlF}	The Jackson Laboratory	Stock No. 004526
Rosa26$^{SmoM2/+}$	The Jackson Laboratory	Stock No. 005130
Gli2^{FlF}	The Jackson Laboratory	Stock No. 007926
Gli3$^{F/F}$	The Jackson Laboratory	Stock No. 008873
hGFAP-Cre	The Jackson Laboratory	Stock No. 004600
Recombinant DNA		
pCAG-Cre	Addgene	#13775

REAGENT or RESOURCE	SOURCE	IDENTIFIER
pCAG-GFP	Addgene	#11150
pCAG-ShhN-Ires-GFP	This Study	N/A
pCAG-ShhN	This Study	N/A
EdU	Life Technologies	E1087
Click-iT EdU Cell Proliferation Kit for Imaging	Invitrogen	C10337
Software and Algorithms		
Cell Ranger	10X Genomics	https://support.10xgenomics.com/single-cell-gene-expression/software/overview/welcome
MACS	Xiaole Shirley Liu's Lab	https://github.com/taoliu/MACS
R	The R Project for Statistical Computing	https://www.r-project.org/
Seurat	Macosko et al., 2015	https://satijalab.org/seurat/
Monocle2	Qiu et al., 2017a, 2017b	https://cole-trapnell-lab.github.io/monocle-release/
GraphPad Prism 5.0	GraphPad	https://www.graphpad.com